JOURNAL OF BIOMOLECULAR STRUCTURE AND DYNAMICS
https://doi.org/10.1080/07391102.2021.1871863

Flavonol morin targets host ACE2, IMP-α, PARP-1 and viral proteins of SARS-CoV-2, SARS-CoV and MERS-CoV critical for infection and survival: a computational analysis

Anamika Gupta[a], Rumana Ahmad[a], Sahabjada Siddiqui[b], Kusum Yadav[c], Aditi Srivastava[a], Anchal Trivedi[a], Bilal Ahmad[d], Mohsin Ali Khan[e], Amit Kumar Shrivastava[f] and Girish Kumar Singh[g]

[a]Department of Biochemistry, Era's Lucknow Medical College and Hospital, Era University, Lucknow, UP, India; [b]Department of Biotechnology, Era's Lucknow Medical College and Hospital, Era University, Lucknow, UP, India; [c]Department of Biochemistry, University of Lucknow, Lucknow, UP, India; [d]Research Cell, Era's Lucknow Medical College and Hospital, Era University, Lucknow, UP, India; [e]Chancellor, Era University, Lucknow, UP, India; [f]Department of Pharmacology, Universal College of Medical Sciences & Hospital, Ranigaon, Bhairahawa, Rupandehi, Nepal; [g]Department of Orthopedics, Era's Lucknow Medical College and Hospital, Era University, Lucknow, UP, India

Communicated by Ramaswamy H. Sarma

ABSTRACT

A sudden outbreak of a novel coronavirus SARS-CoV-2 in 2019 has now emerged as a pandemic threatening to efface the existence of mankind. In absence of any valid and appropriate vaccines to combat this newly evolved agent, there is need of novel resource molecules for treatment and prophylaxis. To this effect, flavonol morin which is found in fruits, vegetables and various medicinal herbs has been evaluated for its antiviral potential in the present study. PASS analysis of morin *versus* reference antiviral drugs baricitinib, remdesivir and hydroxychloroquine revealed that morin displayed no violations of Lipinski's rule of five and other druglikeness filters. Morin also displayed no tumorigenic, reproductive or irritant effects and exhibited good absorption and permeation through GI (clogP <5). In principal component analysis, morin appeared closest to baricitinib in 3D space. Morin displayed potent binding to spike glycoprotein, main protease 3CLPro and papain-like protease PLPro of SARS-CoV-2, SARS-CoV and MERS-CoV using molecular docking and significant binding to three viral-specific host proteins *viz.* human ACE2, importin-α and poly (ADP-ribose) polymerase (PARP)-1, further lending support to its antiviral efficacy. Additionally, morin displayed potent binding to pro-inflammatory cytokines IL-6, 8 and 10 also supporting its anti-inflammatory activity. MD simulation of morin with SARS-CoV-2 3CLPro and PLPro displayed strong stability at 300 K. Both complexes exhibited constant RMSDs of protein side chains and Cα atoms throughout the simulation run time. In conclusion, morin might hold considerable therapeutic potential for the treatment and management of not only COVID-19, but also SARS and MERS if studied further.

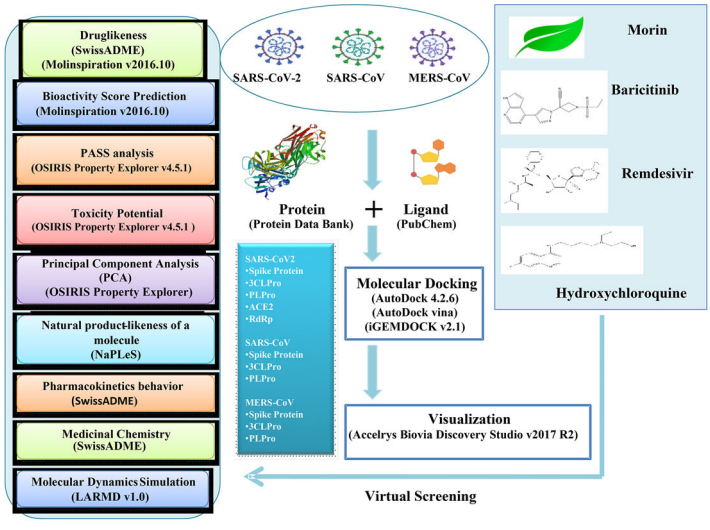

ARTICLE HISTORY
Received 2 September 2020
Accepted 30 December 2020

KEYWORDS
SARS-CoV-2; COVID-19; MERS; SARS; coronaviruses; flavonols; morin; molecular docking

CONTACT Rumana Ahmad rumana_ahmad@yahoo.co.in rahmad@erauniversity.in Department of Biochemistry, Era's Lucknow Medical College & Hospital, Era University, Sarfarazganj, Hardoi Road, Lucknow, UP 226003, India.

Supplemental data for this article can be accessed online at https://doi.org/10.1080/07391102.2021.1871863

Overall view of study

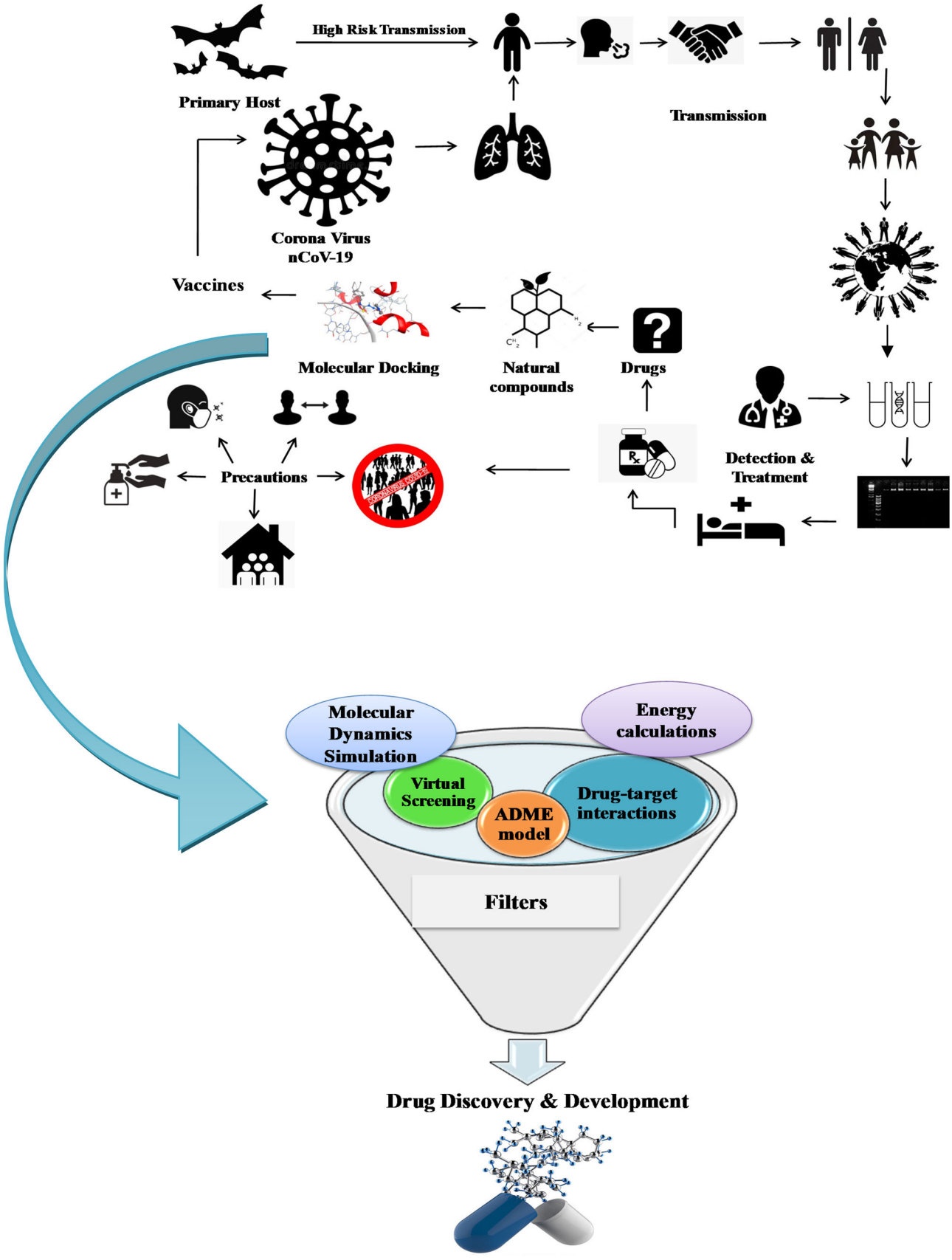

1. Introduction

SARS-CoV-2 is a novel virus currently responsible for acute mortality and morbidity around the world. It was identified at the end of December, 2019 as it emerged during an outbreak in Wuhan, Hubei province, China (Khaerunnisa et al., 2020). This newly evolved virus has caused a pandemic threat to global public health and has been designated as severe acute respiratory syndrome related corona virus SARS-CoV-2 by WHO on February 11, 2020, following guidelines developed with World Organization for Animal Health and Food and Agriculture Organization of the United Nations (Khaerunnisa et al., 2020; https://www.who.int/docs/default-source/coronaviruse/situation-reports/20200121). According to the WHO statistics, globally, there are about 16,114,449 confirmed cases of COVID-19 and about 6,46,641 deaths (as reported on 27 July 2020) (https://www.who.int/emergencies/diseases/novel-coronavirus-2019). The related viral epidemics *viz.* severe acute respiratory syndrome (SARS) and Middle East respiratory syndrome (MERS) also caused by coronaviruses, led to serious public health problems resulting in significant mortality rates in 2003 and 2012, respectively.

Several preventive approaches such as the use of disinfectants, sanitizers, social distancing, quarantine and wearing masks are in vogue against contracting COVID-19, SARS and MERS infections (Abd El-Aziz & Stockand, 2020; Kannan et al., 2020). Despite the preventive and therapeutic strategies undertaken to curb and stall spread of the deadly SARS-CoV-2 in the ongoing global pandemic, the continuing sharp spike in the number of corona positive cases with each passing day points towards the fact that all current preventive and therapeutic options have proven to be insufficient to control the scourge of COVID-19. Therefore, there is an urgent need to find alternative methods/therapeutic options to control the spread of this deadly virus.

Since this novel virus shares 79.6% sequence identity with SARS-CoV and 96.2% overall genome sequence identity to bat CoVs (Zhou et al., 2020), therefore, bats may be considered as primary hosts for this family of viruses which used other animal species as intermediate hosts before finally jumping to humans (Gorbalenya et al., 2020). SARS-CoV-2 has been found to share a nucleotide identity of 89.1% with a bat-like coronavirus (Benvenuto et al., 2020; Wu et al., 2020).

Coronaviruses (CoVs; Supplementary Figure 1.1) belong to the family of *Coronaviridae* (order *Nidovirales*) and have a single stranded positive-sense RNA as genetic material approximately 26–32 kb in size (Abd El-Aziz & Stockand, 2020; Shereen et al., 2020; Weiss & Navas-Martin, 2005). Important structural proteins of SARS-CoV-2 include nucleocapsid protein (N) and envelope protein (E) (Supplementary Figure 1.2). The spike (S) glycoproteins of coronaviruses are the main targets of antibodies as they facilitate entry of SARS-CoV-2 and SARS-CoV *via* binding to high affinity angiotensin-converting enzyme 2 (ACE2) receptor in humans (Liu et al., 2020). The viral invasion process requires S protein priming which is facilitated by the host cell produced serine protease TMPRSS211 (Liu et al., 2020). Genome sequences of the SARS-CoV-2 share more sequence identity in the regions of 1ab polyprotein and spike (S) glycoprotein to SARS-CoV than MERS-CoV (Kannan et al., 2020; Wu et al., 2020). S protein of SARS-CoV-2 has a functional polybasic (furin) cleavage site at the S1–S2 boundary through insertion of 12 nucleotides, which lead to the acquisition of three O-linked glycans around the site.

The viral genome also encodes non-structural proteins (NSPs) including RNA-dependent RNA polymerase (RdRp), coronavirus main protease (3CLpro) and papain-like protease (PLpro) (Báez-Santos et al., 2015; Liu et al., 2020; Ziebuhr et al., 2000). Main protease domain (Mpro) commonly known as 3CL protease has been identified to be a preserved target domain for design of new inhibitors throughout the coronavirus subfamily (Supplementary Figure 1.3).

According to cryo-EM structure analysis, the binding affinity of SARS-CoV-2 spike protein to ACE2 is about 10–20 times higher than that of SARS-CoV S protein (Liu et al., 2020). On the basis of sequence alignment and homology modelling, SARS-CoV and SARS-CoV-2 share a highly conserved receptor-binding domain (RBD) and 76% of sequence similarity in their S proteins. Thus, there is a possibility for development of novel therapeutic agents that can simultaneously target SARS-CoV-2 and SARS-CoV (Chan et al., 2020; Dong et al., 2020; Liu, Morse et al., 2020; Liu, Zhou, et al., 2020; Lu et al., 2020).

Currently, no specific therapy for SARS-CoV-2 is available (Andersen et al., 2020). Thus, considering the severity and magnitude that the ongoing pandemic has attained, there is an urgent need to search and develop novel therapeutic agents to block invasion and/or arrest viral replication in host cell. To this effect, flavonoids which include flavonols, flavones, flavanones and isoflavones, are a large group of naturally occurring phenolic compounds present ubiquitously in nature which can be explored and exploited as therapeutic agents.

In our search towards discovery of a prospective antiviral agent from flavonoids, review of literature revealed the medicinal potential of flavonoid morin in respiratory diseases. Morin (3,5,7,2′,4′-pentahydroxyflavone) is a yellow coloured flavonoid belonging to the group of flavonols found in fruits, vegetables and various medicinal herbs such as figs, mulberry, Osage orange (*Maclura pomifera*), sweet chestnut (*Castanea sativa*), guava (*Psidium guajava* L.) leaves, Brazilian wood (*Chlorophora tinctoria*), almond (*Prunus dulcis*), onion, seaweed, apple, various Chinese and Asian medicinal herbs (Dilshara et al., 2016; Fang et al., 2003; Galvez et al., 2001; Khazan & Hdayati, 2014; Kim et al., 2009; Li et al., 2016; Paoli et al., 2013) and other plants of Moraceae which are used as dietary agents and also as herbal medicines (Chen & Zhang, 2019; Li et al., 2016). Morin is endowed with a wide range of biological activities like anti-inflammatory (Galvez et al., 2001), antiallergen (Kim et al., 2009), hepatoprotective (Lee et al., 2008) antihypertensive, antioxidant, nephroprotective, antidiabetic, anticlastogenic, cytoprotective and has been found to be active against carcinomas of liver, breast, colon and oral cavity (Ciurli et al., 1999; Dilshara et al., 2016; Fang et al., 2003; Galvez et al., 2001; Khazan & Hdayati, 2014; Kim et al., 2009; Lee et al., 2008; Li et al., 2016; Mobley &

Hausinger, 1989; Pal et al., 2015; Paoli et al., 2013; Sujoy & Aparna, 2013).

A study has also revealed the *in vitro* activity of morin against lung cancer cells A549, *via* downregulation of miR-135b (Yao et al., 2017). Additionally, morin has also been found to have a cytoprotective effect in respiratory diseases, cardiovascular disorders and lung cancer *via* its antioxidant and free radical scavenging activity (Lee et al., 2017). Another study has revealed the potential of morin as a bronchodilator and an antitussive agent in treatment of lung disease such as colds, cough and asthma in guinea pigs (Franova et al., 2016).

Since morin has a more or less established role in respiratory diseases, the premise of the present study was its evaluation against the novel SARS-CoV-2 as well as SARS-CoV and MERS-CoV that cause similar and associated respiratory symptoms of pneumonia and lung failure. To further validate our findings on morin, the binding kinetics of morin to selected SARS-CoV-2, SARS-CoV and MERS-CoV proteins was compared to commercially available drugs and repurposed agents known to be effective against COVID-19 *viz.* baricitinib, remdesivir and hydroxychloroquine (HCQ).

The drug baricitinib (brand name Olumiant®) is used for the treatment of rheumatoid arthritis (RA) in adults as it acts as an inhibitor of janus kinase type 1 and 2 (https://clinicaltrials.gov/ct2/show/NCT04320277). The entry of SARS-CoV-2 is facilitated through ACE2 receptor into the host cell. In lungs, alveolar epithelial cells type II (AT2) are prone to viral infections. Disruption of AP2-associated protein kinase 1 (AAK1) may interrupt viral entry and subsequently the virion assembly (Lu et al., 2020; Richardson et al., 2020; Zhao et al., 2020). The safety of use of baricitnib is currently under investigation (https://investor.lilly.com/news-releases/news-release-details/lilly-begins-clinical-testing-therapies-covid-19).

Remdesivir (brand name Veklury®) is an antiviral medication that gets inserted into viral RNA chains, causing their premature termination. It was synthesized and developed by Gilead Sciences in 2017 as a treatment for Ebola virus infection. Remdesivir is an adenosine analog which gets metabolized into its active form GS-441524, that obscures viral RNA polymerase and evades proofreading by viral exonuclease, causing a decrease in viral RNA production. Remdesivir has shown antiviral activity against multiple variants of Ebola virus in cell-based assays (Warren et al., 2016) as well as in a rhesus monkey model of Ebola virus disease (Warren et al., 2015). An *in vitro* study has shown that remdesivir can inhibit SARS-CoV and MERS-CoV replication (Boseley, 2020). Currently, WHO has reported failure in safe use of remdesivir in clinical trials for treating SARS-CoV-2 patients (Boseley, 2020). There is need for more research to elucidate the mechanism of action and safety of the drug.

The gravity of the ongoing pandemic has spawned several drug discovery programs to search for novel drugs not only from natural and synthetic sources but also evaluation of pre-existing drugs for their prospective antiviral activity and repurposing/repositioning them as novel antiviral agents against SARS-CoV-2. In recent clinical trials, HCQ and chloroquine (CQ), have been found to be effective against novel SARS-CoV-2 *in vitro*, thus, further broadening their therapeutic spectrum and cementing their role as repositioned drugs (Costedoat-Chalumeau et al., 2015; Ferner & Aronson, 2020). Currently, clinical trials of HCQ in combination with other drugs are being used in SARS-CoV-2 treatment. Though HCQ is generally considered safe and side-effects are generally mild with no secondary or associated complications, both HCQ and CQ have been found to be toxic in SARS-CoV-2 patients with cardiovascular disorders (Frisk-Holmberg et al., 1983; Touret & de Lamballerie, 2020). Recently, a clinical trial for the safety of use of CQ and remdesivir for treatment of SARS-CoV-2 *in vitro* has been done (Wang et al., 2020). Remdesivir and CQ potently blocked virus infection at low-micromolar concentration and displayed a high selectivity and low cytotoxicity index against Vero E6 cells. Interestingly, CQ has been found to be active against SARS-CoV (Keyaerts et al., 2009), SARS coronavirus OC43 (Keyaerts et al., 2004), ebolavirus (Dowall et al., 2015), Nipah virus (Pallister et al., 2009), influenza virus (Vigerust & McCullers, 2007), chikungunya virus (CHIKV) (Coombs et al., 1981; Falzarano et al., 2015), enterovirus EV-A71 (Delogu & de Lamballerie, 2011) and Zika virus (Tan et al., 2018). However, the associated toxicity effects have so far limited the use of CQ as an antiviral agent in clinical trials.

In the present study, an attempt has been made to investigate the molecular interaction of selected SARS-CoV-2, SARS-CoV and MERS-CoV target proteins with morin, a naturally occurring flavonoid, *vis-à-vis* commercially available antiviral drugs using molecular docking. The feasibility of morin to behave as an antiviral candidate was assessed using a number of filters.

2. Materials and methods

2.1. PASS analysis

The present study was carried out at Molecular Chemoinformatics Section, Cell and Tissue Culture Lab, Dept. of Biochemistry, Era's Lucknow Medical College and Hospital, Era University, Lucknow. Flavonol morin was selected for its ability to obey Lipinski's rule of five, Ghose, Veber, Egan and Muegge filters for druglikeness of a candidate compound as well as on the basis of previously reported structure activity relationships (SARs) *vis-à-vis* commercial synthetic drugs *viz.* baricitinib, remdesivir and HCQ for the present study (Dolinsky et al., 2007; Dong et al., 2020; Egan et al. 2000; Faber et al., 2005; Fang et al., 2003; Ferner & Aronson, 2020; Ferriola et al., 1989; Franova et al., 2016).

PASS analysis was performed using OSIRIS Property Explorer version 4.5.1 (http://www.openmolecules.org/propertyexplorer/index.html). This online PASS (Prediction of Activity Spectra for Substances) software predicts biological activities, pharmacological activity and mechanism of action of chemical compounds on the basis of structure-activity relationship (Ahmad, 2019).

2.2. Druglikeness evaluation

Lipinski's rule of five (RO5) is used to evaluate druglikeness of a chemical compound possessing properties that would make it a likely or potential drug in humans. Based on a set of counting rules, it is an important scale used for lead optimization. A molecule is found to obey Lipinski's rule if: (1) its molecular weight $\leq$500 (2) the calculated logarithm of the octanol-water partition coefficient (cLogP) $\leq$5 (3) hydrogen bond donor atoms $\leq$5 (4) the sum of the number of nitrogen and oxygen atoms $\leq$10. In general, an orally active drug has no more than one violation of the given criteria. Lipinski's rule of five is helpful in describing molecular properties of drug compounds required for estimation of important pharmacokinetic parameters such as absorption, distribution, metabolism and excretion (ADME) (Khan et al., 2018; Lipinski et al., 1997). Druglikness was further evaluated using SwissADME software which follows different set of rules including Lipinski's (Pfizer) (Ursu et al., 2011), Ghose (Amgen) filter (Ghose et al., 1999), Veber (GSK) rule (Veber et al., 2002), Egan (Egan et al., 2000) and Muegge (Bayer) filters (Muegge et al., 2001).

2.3. Bioactivity score prediction

Molinspiration version 2016.10, an online web tool was used to predict the bioactivity score of morin with respect to selected SARS-CoV-2, SARS-CoV and MERS-CoV proteins *vis-à-vis* commercially available antiviral drugs. Drug score values are useful in indicating overall medicinal potential of a prospective compound as a drug candidate. If the bioactivity drug score is $>$0.0, then the compound is active; values between $-$5.0 and 0.0 indicate compound is moderately active and values <-5.0 are indicative of an inactive compound (Ahmad, 2019; Martin, 2005; Verma, 2012). Higher the bioactivity score, the greater is the probability that the compound under investigation would be active and possess pharmacological activities in clinical trials. Molinspiration software was also used to find the number of rotatable bonds, H-bond acceptors and H-bond donors.

2.4. Toxicity potential assessment

The prediction of toxicity of candidate drugs is an early and vital step in drug discovery and development process. Morin was computationally screened for any mutagenic, tumorigenic, irritant and reproductive toxicity risks. Toxicity index of morin *vis-a-vis* commercially available antiviral drugs was generated and analyzed using OSIRIS Data Warrior software version 4.5.1 (http://www.openmolecules.org/datawarrior/) (Ahmad, 2019).

2.5. Natural product-likeness assessment

Natural product-likeness (NPL) assessment was performed using online computed NaPLeS software. Natural product-likeness of a molecule is the overall similarity of the selected molecule to the structure space covered by natural products. This tool is useful in screening compound libraries and in designing target compounds (Ertl et al., 2008; Jayaseelan et al., 2012).

2.6. Pharmacokinetics behaviour assessment

ADME behavior of morin *vis-à-vis* commercially available antiviral drugs was evaluated using SwissADME software. The software evaluates lipophilicity and polarity of small molecules through several parameters including blood brain barrier (BBB), skin permeability, gastrointestinal absorption and Cytochromes P450 isoenzymes (CYPs) (Daina et al., 2017).

2.7. Brain Or IntestinaL EstimateD permeation analysis

Gastrointestinal absorption and brain barrier access are the two main pharmacokinetic behaviors important to estimate during evaluation of drug candidates for development. Brain Or IntestinaL EstimateD permeation (BOILED-Egg) predictive model works by enumerating the lipophilicity and polarity of small molecules for bioavailability. This prediction was performed using SwissADME software in which morin and the four antiviral drugs were subjected to lipophilicity (WLOGP) and polarity (TPSA) computation (1) in drugs SMILES notation (Daina & Zoete, 2016).

2.8. SwissADME analysis

This software implements PAINS (Baell & Holloway, 2010), Brenk filters (Brenk et al., 2008), Lead-likeness (Teague et al., 1999) and Synthetic accessibility (SA) (Ertl & Schuffenhauer, 2009) scores for predicting the druglikeness of candidate compounds and is used for high throughput screening (HTS) of physiochemical properties of compounds at early stages of drug development.

ADMET, druglikeness and toxicity properties of morin *versus* standard drugs were also analyzed using PreADMET ver 2.0 (https://preadmet.bmdrc.kr/).

2.9. Bioavailability radar

The drug-likeness of a molecule can be virtually defined from the Bioavailability radar plot or 'spider' or 'cobweb' plot. The pink colored zone is suitable for oral bioavailability, and the molecular radar plot must fall entirely within the zone to be considered a drug-like molecule. Six physicochemical properties are taken into account *viz.* lipophilicity, size, polarity, solubility, flexibility and saturation, to fall within the pink zone (Lovering et al., 2009; Ritchie et al., 2011).

2.10. Swiss target prediction analysis

The probability of morin to behave as a GPCR ligand, ion-channel modulator, kinase inhibitor, nuclear receptor ligand, protease and enzyme inhibitor in biological systems *vis-à-vis* commercially available antiviral drugs was evaluated

using Swiss Target Prediction software (http://www.swisstargetprediction.ch) (Daina et al., 2017).

2.11. Principal Component Analysis

Principal component analysis (PCA) of morin *vis-à-vis* commercially available antiviral drugs was performed using Osiris Property Explorer 4.5.1 for multi-dimensional property spaces visualization by assigning dimensions to numerical descriptor properties *viz.* MW, % Absorption and TPSA. The bar charts and 3D scatter plots of principal components were made in OSIRIS Property Explorer 4.5.1 (http://www.openmolecules.org/propertyexplorer/index.html) and Accelrys Biovia Discovery Studio version 2017 R2, respectively (Ahmad, 2019), to depict the behavior and position of morin *versus* commercially available antiviral drugs in chemical 3D space on the basis of the above-mentioned properties.

2.12. Molecular docking

2.12.1. Ligand Preparation

PubChem database were used to retrieve 3D structures of morin and three antiviral drugs (baricitinib, remdesivir and HCQ) in SDF format (Figure 1). Prior to docking, ligands were subjected to energy minimization using Merck Molcular Force Field (MMFF94). All ligand structures underwent structural optimization using AutoDock Tools (ADT) version 4.2.6. (Ahmad, 2019; Khan et al., 2018)

2.12.2. Target protein preparation

The 3D crystal structures of respective target receptors/proteins of SARS-CoV-2, SARS-CoV and MERS-CoV (whose X-ray diffraction structures are available in RCSB database) were downloaded from Protein Data Bank (http://www.rcsb.org/pdb) in PDB format. All protein structures were subjected to refinement before docking analyses as reported previously (Ahmad, 2019). For visualization purpose, Accelrys Biovia Discovery Studio version 2017 R2 (Biovia, San Diego, CA) was used (Ahmad, 2019; Khan et al., 2018)

The PDB IDs of the target proteins of SARS-CoV-2 (Supplementary Figure 2.1) were as follows: HR2 domain of S2 subunit (PDB ID: 6LVN), post-fusion core of S2 subunit (PDB ID: 6LXT), Nucleocapsid protein (PDB IDs: 6M3M and 6VYO), Spike glycoprotein (PDB IDs: 6VYB and 6VXX), ACE2 Receptor (PDB IDs: 1O8A, 6LZG and 6M0J), RdRp (RNA dependent RNA polymerase; PDB ID: 6M71), NSP9 (PDB ID: 6W4B), 3CLPro (PDB ID: 6Y84, 6LU7, 6Y2E and 6M03), papain-like protease (PLPro) (PDB ID: 6W9C).

Target human proteins (Supplementary Figure 2.1) were as follows: human importin-alpha1 (PDB ID: 3WPT), poly (ADP-ribose) polymerase (PARP)-1 (PDB ID: 5DS3), IL-6 (PDB ID: 1ALU), IL-8 (PDB ID: 1IL8), IL-10 (PDB ID: 2H24) and human ACE receptor protein (PDB ID: 1O8A)

The PDB IDs of the target proteins of SARS-CoV (Supplementary Figure 2.2) were as follows: 3CLPro (PDB IDs: 2DUC, 1UJ1 and 1Z1J), papain-like protease (PDB ID: 2FE8), Spike glycoprotein (PDB ID: 5WRG, 5XLR and 1WNC).

The PDB IDs of the target proteins of MERS-CoV (Supplementary Figure 2.3) were as follows: papain-like protease (PDB IDs: 4RNA and 4PT5), Spike Glycoprotein (PDB IDs: 5X5C, 5X5F and 4L3N).

2.12.3. Analysis of binding kinetics of morin with respect to selected SARS-CoV-2, SARS-CoV and MERS-CoV proteins versus known antiviral drugs

The optimized structures of morin and the four known antiviral drugs were subjected to molecular docking analysis against selected SARS-CoV-2, SARS-CoV and MERS-CoV target proteins using Autodock version 4.2.6, a free, automated software developed by Molecular Graphics Lab, Scripps Research Institute, La Jolla, CA (http://autodock.scripps.edu/). The best docking orientations were subsequently analyzed using Accelrys Biovia Discovery Studio version 2017 R2 and PyMol. The docking software calculates the binding energies and K_d values of ligands to target proteins (Ahmad, 2019; Khan et al., 2018).

2.12.4. Validation of docking analysis

The best docking results obtained for morin with respect to SARS-CoV-2, SARS-CoV and MERS-CoV target proteins were further validated using two additional docking softwares *viz.* AutoDock Vina (Trott & Olson, 2010) and iGEMDOCK v 2.1 (Yang & Chen, 2004).

2.13. Molecular dynamics simulation

Protein dynamics is fundamental to all biological processes, including transmission of molecular signals, cell cycle regulation and enzymatic catalysis. In-depth analysis of ligand-driven protein molecular dynamics leads to an optimal understanding of protein functioning within a biological system, which is needed for drug discovery.

Web server LARMD version 1.0 (http://chemyang.ccnu.edu.cn/ccb/server/LARMD/) is a new online application available freely to access for investigating receptor-ligand interactions and dynamics at atomic level based on the three modules *viz.* conventional molecular dynamics (Int_mod), normal mode analysis (Nor_mod) and steered molecular dynamics simulations (Str_mod). The widely used softwares such as CAVER3.0, AMBER16, MDTraj and Bio3d are integrated into these three modules. To visualize and analyze the result on the Web page, the plugins and software, such as JSmol, Chart.js and MolScript are integrated (Yang et al., 2020a).

In separate studies, the best binding poses of morin with two SARS-CoV-2 target proteins *viz.* main protease 3CLPro (PDB ID 6Y84) and papain-like protease PLPro (PDB ID 6W9C), generated using molecular docking were uploaded in the first step on PDB2PQR server which prepared electrostatic fields of the receptor under different pH values. Advanced options were customized for MD simulation time of 4 ns. After submission of the ligand-receptor complex file, the second step involved enlisting of ligand and nonstandard residue(s) for energy calculations and trajectory analysis before the final job

submission. The server returned the molecular dynamics simulation results in the form of components including PCA, conformation cluster, dynamic residue cross-correlations, hydrogen bond analysis, free energy of binding and energy decomposition. Viral protein-ligand interaction and dynamics was studied at atomic level using the conventional molecular dynamics simulation module (Int_mod), and steered molecular dynamics simulation module (Str_mod) (Dolinsky et al., 2007; Yang et al., 2020a).

3. Results

3.1. PASS analysis

The molecular properties of morin *versus* four antiviral and one antibacterial drug are summarized in Table 1. The values of clogP, MW, druglikeness, TPSA, % absorption, Lipinski's violations, hydrogen bond donor and acceptor obtained for morin were compared with the above-mentioned drugs. The clogP (logarithm of partition coefficient between n-octanol and water) value is a measure of the hydrophilicity of a compound (Meanwell, 2016). Low hydrophilicity values and, therefore, high logP values indicate poor absorption or permeation of the compounds. For being well absorbed in biological system, the compounds must have clogP value not greater than 5.0 (Kaiser & Valdmanis, 1982). In the present study, morin and all standard drugs were found to have a clogP value of <5 which is an indicator of good absorption and permeation through GI tract. For a drug to be effective, the MW of the candidate drug should be <500 (Behera et al., 2014). Compounds with high MW are less likely to be absorbed and reach their site of action in a biological system. The results obtained clearly indicated that morin displayed no violations of Lipinski's rule of fve as compared to remdesvir and azithromycin which had 2 violations each of Lipinski's rule of five. This means that morin conformed to all the physiochemical parameters for a candidate to behave as an ideal drug.

3.2. Bioactivity and bioavailability scores and prediction of druglikeness

Drug score values indicate overall potential of a prospective compound to behave as a drug. Molinspiration version 2016.10 was used to evaluate the bioactivity scores of morin and reference drugs with respect to human receptors like GPCRs, ion channels, nuclear receptors and enzymes like proteases and kinases (Ahmad, 2019). As a general rule, if the BAS is >0.0, then the drug candidate is physiologically active; if it is in the range -5.0 to 0.0; then the drug candidate is moderately active, and if the BAS <-5.0, then the drug candidate is inactive. BAS scores for morin as a GPCR ligand, ion channel modulator, kinase inhibitor, nuclear receptor ligand and protease inhibitor were found to be >-5.0, thereby proving its bioactivity. Interestingly, morin displayed considerable activity as an enzyme inhibitor as is evident from its positive BAS of >0.0 (i.e., 0.28), thus supporting its role as a potential viral protease inhibitor.

Druglikeness is a qualitative property of molecules whose positive value for a molecule indicates that the molecule predominantly contains fragments which are frequently present in commercial drugs (Ursu et al., 2011). Druglikeness decreased in the following order: azithromycin > HCQ > morin > baricitinib > remdesivir (Table 2).

SwissADME software also predicts the qualitative probability for a molecule to behave as an oral drug in relation to its bioavailability score (ABS). The software uses a set of five filters to define druglike properties of compounds. The filters include Lipinski (Pfizer) (Ursu et al., 2011), Ghose (Amgen) (Ghose et al., 1999), Veber (GSK) (Veber et al., 2002), Egan (Pharmacia) (Egan et al., 2000) and Muegge (Bayer) (Muegge et al., 2001). Multiple evaluations allow solidarity in selection of druglike molecules. Violations of filters indicate an unfit drug candidate. In the present study, morin, baricitinib and HCQ were found to obey all filters with no violations. The Abbot Bioavailability Score (ABS) predicts the bioavailability of promising drug candidates at an early phase of drug development process (Martin, 2005). The potential drug must possess $>10\%$ oral bioavailability in rats. Morin, baricitinib and HCQ were found to obey all the five filters and had ABS scores of 0.55 as compared to other reference drugs indicating their feasibility to be administered orally (Table 3).

Protein target prediction of morin *versus* reference drugs was *also* done using SwissADME. Figure 2 depicts the % bioactivity of morin and reference drugs with respect to selected protein targets *viz*. enzymes, kinases, oxidoreductases, phosphatases, proteases, phosphodiesterases and lyases. Results showed that morin displayed maximum activity as an enzyme (26.7%) and kinase (13.3%) ligand.

3.3. Toxicity potential evaluation

Computational methods also predict hazardous effects such as toxicity of candidate drug molecules and other chemicals. These unsuitable molecules are removed from drug screening as they can have harmful effects on biological systems. In the present study, morin was evaluated for its toxic effects against parameters *viz*. mutagenic, tumorigenic, reproductive and irritant effects *versus* reference drugs by using pre-computed set of structural fragments in Data warrior (OSIRIS) software. Remdesivir and HCQ were found to be associated with potent mutagenic, tumorigenic, reproductive and irritant effects (Table 4). Morin displayed no tumorigenic, reproductive or irritant effect. However, it was found to be mutagenic indicating the need for modification of its structure-activity relationship (SAR) for decreasing its mutagenicity (Table 4).

3.4. Natural product-likeness assessment

Natural products have tremendous potential as a source of novel and unique drugs and other bioactive synthetic products owing to their bioactivity that is a result of evolutionary optimization for effective interactions with biological

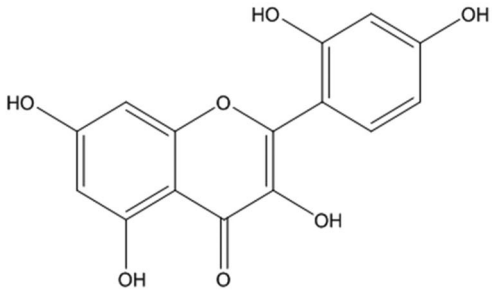

Morin

PubChem CID: 5281670

Molecular Formula: $C_{15}H_{10}O_7$

Molecular Weight: 302.23 g/mol

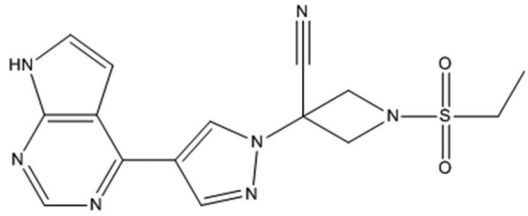

Baricitinib

PubChem CID: 44205240

Molecular Formula: $C_{16}H_{17}N_7O_2S$

Molecular Weight: 371.4 g/mol

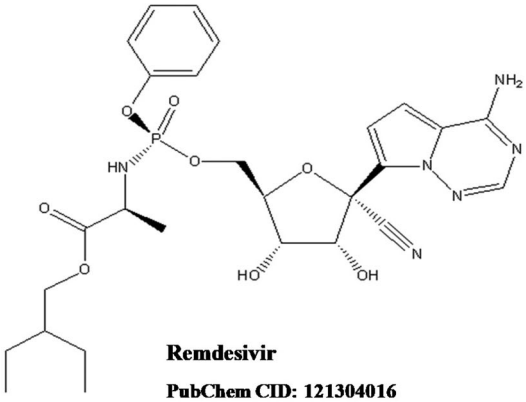

Remdesivir

PubChem CID: 121304016

Molecular Formula: $C_{27}H_{35}N_6O_8P$

Molecular Weight: 602.6 g/mol

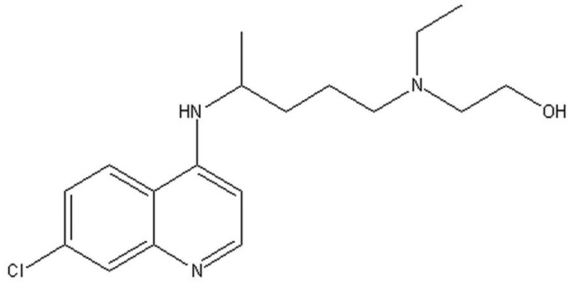

Hydroxychloroquine

PubChem CID: 3652

Molecular Formula:$C_{18}H_{26}ClN_3O$

Molecular Weight: 335.9 g/mol

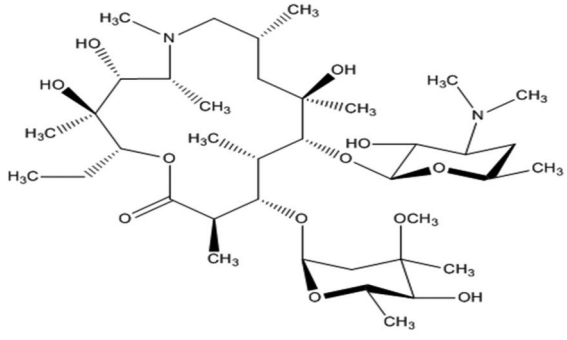

Azithromycin

PubChem CID: 447043

Molecular Formula: $C_{38}H_{72}N_2O_{12}$

Molecular Weight: 749 g/mol

Figure 1. Chemical structures of the ligands used in the study.

receptors. The evaluation of the compound NP-likeness is an important asset in the selection and optimization of NP-like drugs and synthetic bioactive compounds. In 2008, Ertl et al. suggested a natural product (NP) likeness score, which, for a given molecule, is its similarity to the structure space covered by NPs compared to the structure space covered by synthetic molecules (SM). NPL scores are used to prioritize compounds from virtual libraries and are based on the sum

Table 1. PASS analysis of morin *versus* reference drugs (baricitinib, remdesivir, HCQ and azithromycin) calculated by OSIRIS Property Explorer.

Physicochemical parameters										
Lipinski's rule of five										
S. No.	Ligand	%Absorption (>50%)[a]	Topological polar surface area (Å)^2 (TPSA)[b] (<160 Å)	MW (<500)	c log P (<5)[c]	Heavy atom count	Hydrogen bond donors (nOHNH) (≤5)	Hydrogen bond acceptors (nON) (≤10)	Number of rotatable bonds (≤10)	Lipinski's violation
1	Morin	63.69	131.35	302.23	1.490	22	5	7	1	0
2	Baricitinib	67.40	120.57	371.43	0.971	26	1	9	5	0
3	Remdesivir	38.77	203.57	602.59	0.304	42	5	14	42	2
4	HCQ	92.31	48.38	335.88	3.082	23	2	4	9	0
5	Azithromycin	46.87	180.09	749.00	1.656	52	5	14	7	2

[a]Percentage Absorption was calculated as: % Absorption = 109 − [0.345* Topological Polar Surface Area].
[b]Topological polar surface area (defined as a sum of surfaces of polar atoms in a molecule).
[c]Logarithm of compound partition coefficient between n-octanol and water.

Table 2. Bioactivity score and Druglikeness of morin *versus* reference drugs calculated by Molinspiration.

S. No.	Ligand	GPCR ligand	Ion channel modulator	Kinase inhibitor	Nuclear receptor ligand	Protease inhibitor	Enzyme inhibitor	Druglikeness
1	Morin	−0.09	−0.22	0.22	0.34	−0.27	0.28	−0.082
2	Baricitinib	0.27	−0.12	0.62	−0.76	−0.03	0.11	−2.921
3	Remdesivir	0.27	−0.35	0.20	−0.48	0.49	0.38	−21.38
4	HCQ	0.35	0.30	0.44	−0.12	0.12	0.15	5.726
5	Azithromycin	−0.60	−1.50	−1.35	−1.40	−0.28	−0.82	13.854

Table 3. Druglikeness and Abbot Bioavailability Score of morin *versus* reference drugs calculated using SwissADME.

S. No.	Druglikeness	Morin	Baricitinib	Remdesivir	HCQ	Azithromycin
1	Lipinski's rule	Yes (0 violations)	Yes (0 violations)	No (2 violations) *MW* > 500 Nor >10	Yes (0 violations)	No (2 violations) *MW* > 500 Nor >10
2	Ghose filter	Yes	Yes	No (3 violations) *MW* > 480 *MR* > 130 #atoms > 70	Yes	No (3 violations) *MW* > 480 *MR* > 130 #atoms > 70
3	Veber rule	Yes	Yes	No (2 violations) Nor > 10 TPS*A* > 140	Yes	No (1 violation) TPSA > 140
4	Egan filter	Yes	Yes	No (1 violation) TPSA >131.6	Yes	No (1 violation) TPSA >131.6
5	Muegge filter	Yes	Yes	No (3 violations) *MW* > 600 TPS*A* > 150 H-acc >10	Yes	No (3 violations) *MW* > 600 TPS*A* > 150 H-acc >10
6	Bioavailability score (ABS)*	0.55	0.55	0.17	0.55	0.17

Nor: No. of rotatable bond; MW: molecular weight; MR: molar refractivity; #atoms: atom count; TPSA: topological polar surface area; H-acc: hydrogen bond acceptor.
*Bioavailability Score (ABS): 0.55 (obeys all 5 filters) and 0.17 (violates filters).

of the frequency of their fragments among NPs and SMs. Here the fragments are represented by atom signatures that are canonical circular descriptors of an atom's environment in the molecule.

NaPLeS is a web application that allows enumerating the NP-likeness score online (http://naples.naturalproducts.net) NaPLeS has a database comprising 364,807 unique natural products and 489,780 unique synthetic molecules, unified on the basis of structural identity and ignoring stereochemistry. The score for synthetic molecules ranges between −3.61 and 4.01 with an average of −0.61. The score for natural products is distributed between −2.31 and 5.15 with an average of 1.48. In the present study, the NPL score of morin was found to be well within the range for natural products i.e., 1.75 with a heavy atom count of 22 (Table 5 and Figure 3) as compared to reference drugs.

3.5. Assessment of pharmacokinetic properties

It is evident from Table 1 that owing to its low MW (302.3), morin is unlikely to be digested further and capable of being absorbed from GI tract rapidly, thereby increasing its plasma concentration and bioavailability. Baricitinib and HCQ were also predicted to have high GI absorption as compared to remdesivir and azithromycin. Inability to cross the BBB can help in reducing the side effects and toxicity of drugs to brain or improve the efficacy of drugs whose

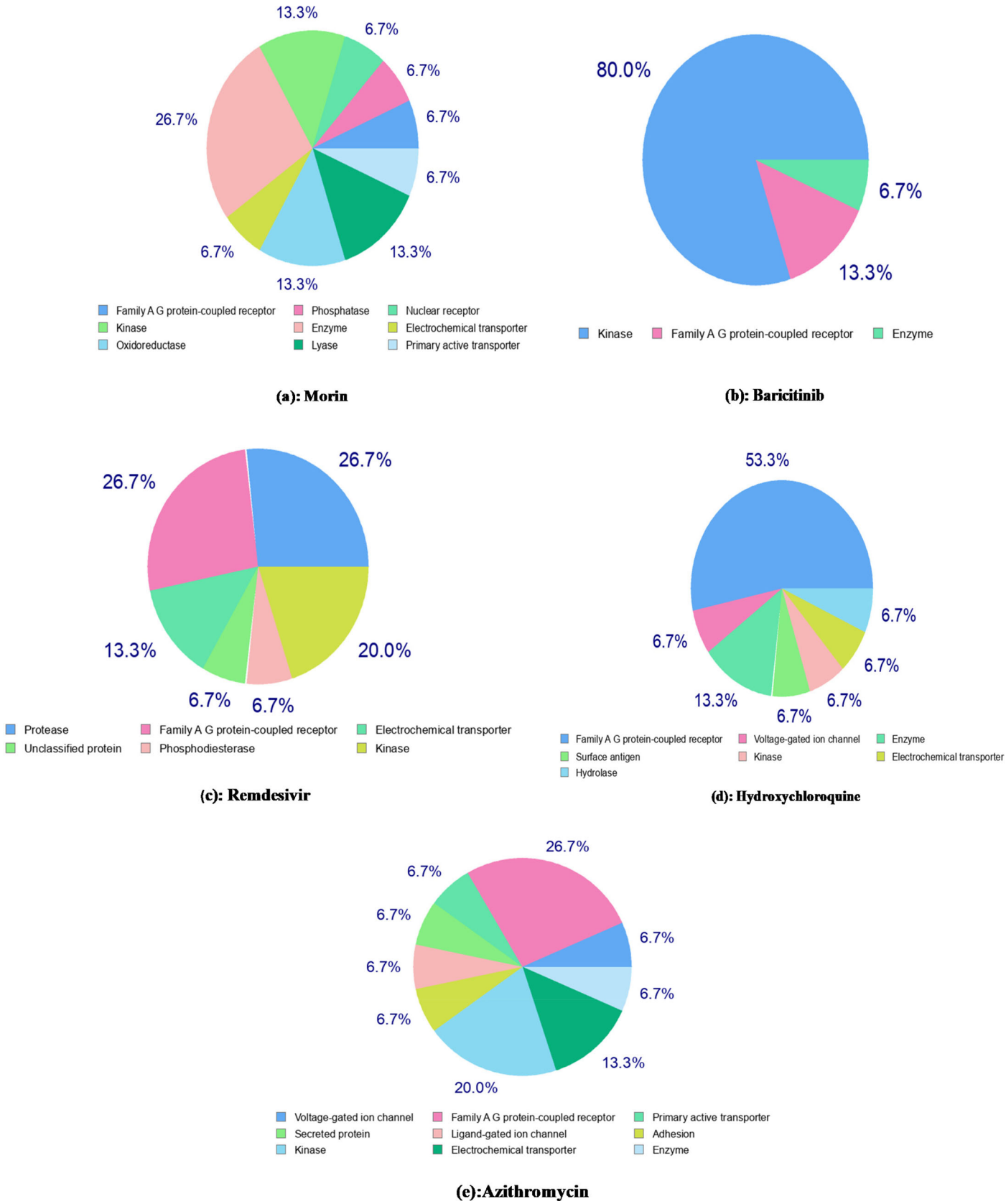

Figure 2. Frequency of protein target prediction of morin *versus* reference drugs as shown in the pie chart and calculated by SwissTarget Prediction (SwissADME).

pharmacological target of action is outside the brain (Aniyery et al., 2015). Morin was found to be incapable of penetrating the BBB along with baricitinib, remdesivir and azithromycin *versus* HCQ which showed a high BBB permeability. Morin was also predicted to have low topical absorption like other reference drugs. Unlike baricitinib, remdesivir and azithromycin, morin and HCQ were predicted *not* to behave as P-gp substrates, and hence, unlikely to be pumped out of the cell

Table 4. Toxicity calculations of morin *versus* reference drugs calculated by Osiris Property Explorer.

S. No.	Ligand	Mutagenic	Tumorigenic	Reproductive effective	Irritant
1	Morin	High	None	None	None
2	Baricitinib	None	None	None	None
3	Remdesivir	None	High	High	High
4	HCQ	High	None	None	None
5	Azithromycin	None	None	None	None

Table 5. NPL Scores and Heavy atom counts of morin *versus* reference drugs calculated using NaPLeS web application.

S. No.	Ligand	NPL score	Heavy atom count
1	Morin	1.75	22
2	Baricitinib	−0.37	26
3	Remdesivir	0.97	42
4	HCQ	0.10	23
5	Azithromycin	1.93	52

by the glycoprotein, thus lessening the probability of cells developing resistance towards them. On the other hand, morin and HCQ were predicted to behave as CYP1A2 inhibitors, and thus, were less susceptible to be metabolized and rendered inactive by the enzyme as compared to the other four reference drugs. Morin and HCQ were also predicted to be CYP2D6 and CYP3A4 inhibitors which points towards their decreased elimination and metabolism by these enzymes and hence increased plasma concentrations as opposed to baricitinib, remdesivir and azithromycin. However, morin and none of the reference drugs were predicted to behave as CYP2C19 inhibitors (Table 6).

Interestingly, the serum half lives of morin and reference drugs were found to decrease in the following order: HCQ < azithromycin < baricitinib < remdesivir < morin (Table 6). Additional analysis of ADMET, druglikeness and toxicity properties of morin *versus* standard drugs using PreADMET version 2.0 have been presented as Supplementary Table S3 parts A, B, and C.

3.6. Brain Or IntestinaL EstimateD permeation analysis

The BOILED-Egg model (Brain Or IntestinaL EstimateD permeation model) was *also* used to assess the gastrointestinal (GI) absorption and blood brain barrier (BBB) permeability of morin *versus* reference drugs (Daina et al., 2017). Boiled egg plot was obtained using SwissADME (Figure 4). The white region depicts the physicochemical space of molecules with highest probability of being absorbed by the GI tract, and the yellow region (yolk) depicts the physicochemical space of molecules with highest probability to permeate to the brain (Daina & Zoete, 2016). The results obtained were identical to those given in Table 6. Morin and baricitinib were found to have highest probability of being absorbed by GI and HCQ was found to have good brain access.

3.7. High throughput screening (HTS) analysis using SwissADME

HTS is employed in drug discovery programs for screening biochemical parameters of drug-like compounds. Pan Assay Interference Compounds (PAINS) are chemical compounds that often give false positive biological results during HTS (Baell & Holloway, 2010). Structural Alert acknowledged by Brenk alert (Brenk et al., 2008) informs that a particular drug is toxic, metabolically unstable, chemically reactive and lacks good pharmacokinetic properties. In drug discovery, potent compounds are prone to conflict with optimum ADME parameters. Lead selection criteria are subjected to HTS during drug development (Teague et al., 1999). Lead-likeness is a set of rules based on biochemical screening filters (Hann & Keserü, 2012). In computer-aided drug design (CADD), synthetic accessibility (SA) score is a key parameter in selecting the potential drug-like molecule (Ertl & Schuffenhauer, 2009). SwissADME software is often used to evaluate SA of druglike molecule which is characterized as a score between 1 (easy to synthesize) and 10 (very difficult to synthesize). Table 7 depicts the biochemical properties of morin *versus* reference drugs. Morin was found to obey PAINS, Brenk and leadlikeness filters with a SA score of 3.25, thus, making it as a feasible drug candidate whereas HCQ displayed two violations of leadlikeness rules though having a good SA score of 2.82.

3.8. Bioavailability radar

From the SwissADME prediction software, it is evident that HCQ and baricitinib have the optimal range of all the mentioned six properties, enabling them to possess considerable chemotherapeutic potential. Morin failed to obey only saturation property, whereas remdesivir failed to obey more than one property (Figure 5, Table 8).

3.9. Principal Component Analysis

PCA was carried out using physicochemical properties showing maximum variability between morin *versus* reference drugs *viz.* TPSA, % absorption and MW, using linear correlation between variables (Figure 6a,b). Morin appeared closest to baricitinib in chemical 3-D space on the basis of its similarity to baricitinib in physicochemical properties. Table 9 represents the Bravais-Pearson (linear correlation) coefficient of morin *versus* reference drugs for physicochemical properties.

3.10. Molecular docking

Tables 10–12 depict the docking results of morin *versus* reference drugs with respect to target viral proteins of SARS-CoV-2, SARS-CoV and MERS-CoV, respectively, calculated using AutoDock version 4.2.6.

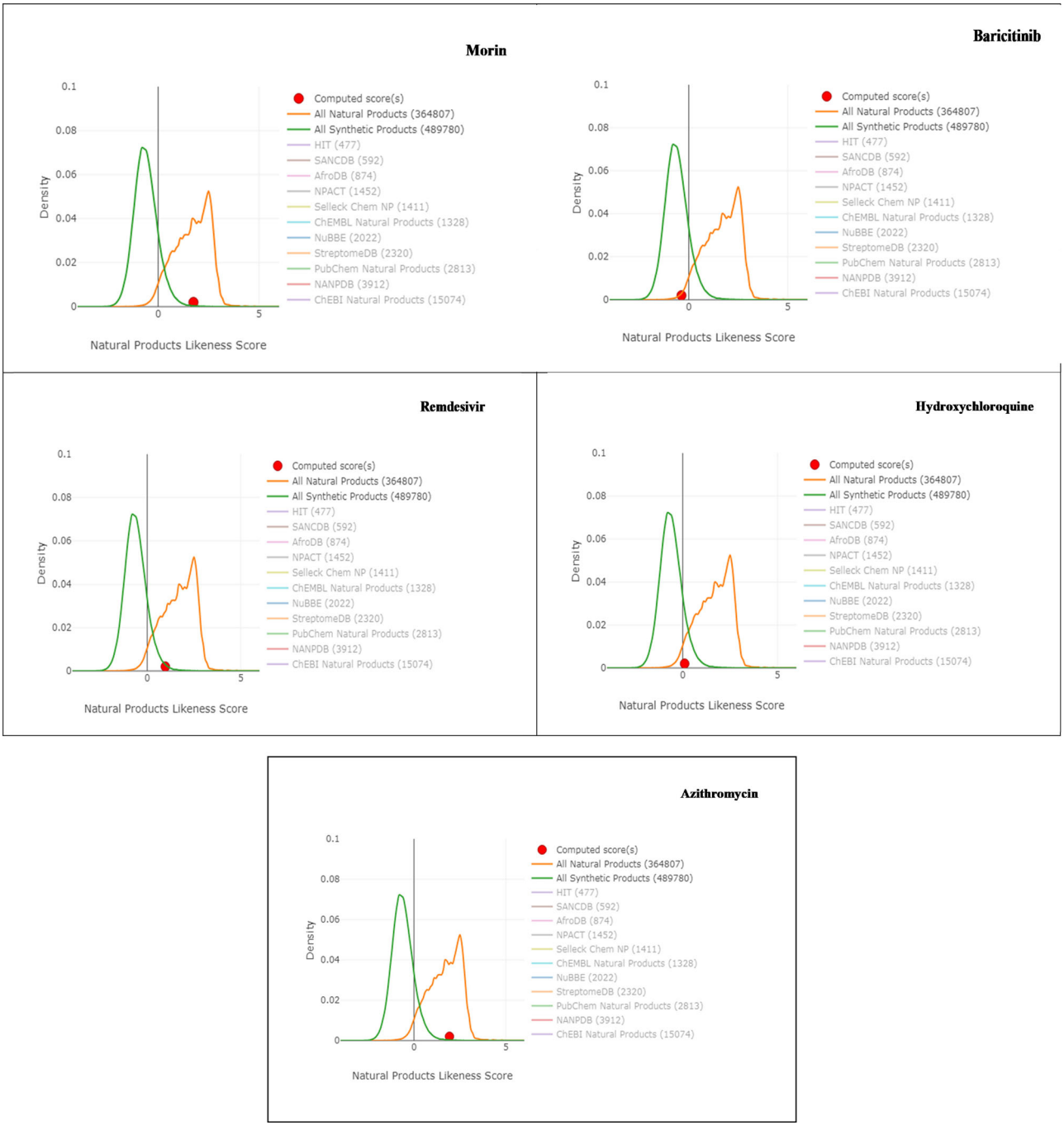

Figure 3. Comparison of NPL scores of morin and reference drugs with those of compounds present in NaPLeS database.

Table 6. Evaluation of pharmacokinetic parameters of morin *versus* reference drugs using SwissADME.

S. No.	Pharmacokinetic property	Morin	Baricitinib	Remdesivir	HCQ	Azithromycin
1	GI absorption	High	High	Low	High	Low
2	BBB permeant	No	No	No	Yes	No
3	P-gp substrate	No	Yes	Yes	No	Yes
4	CYP1A2 inhibitor	Yes	No	No	Yes	No
5	CYP2C19 inhibitor	No	No	No	No	No
6	CYP2C9 inhibitor	No	No	No	No	No
7	CYP2D6 inhibitor	Yes	No	No	Yes	No
8	CYP3A4 inhibitor	Yes	No	Yes	No	No
9	Log Kp (skin permeation)	−7.05 cm/s	−8.89 cm/s	−8.62 cm/s	−5.81 cm/s	−8.01 cm/s
10	Serum Half-life ($T^1/_2$)	0.37 h	12.5 h	0.39 h	537 h	68 h

GI absorption: gastrointestinal absorption; BBB: blood-brain barrier; P-gp : P-glycoprotein ; CYP: Cytochrome P450 .

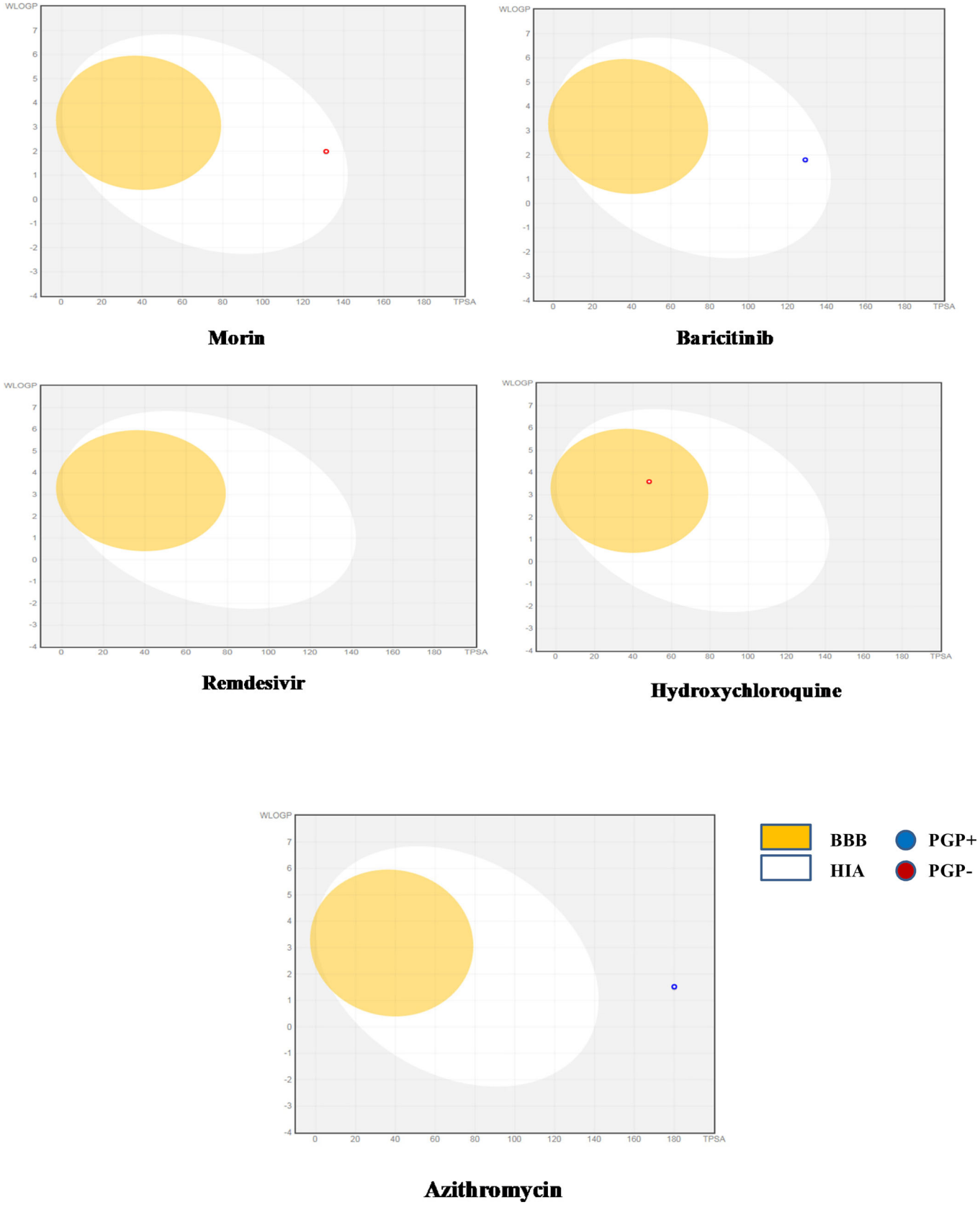

Figure 4. Boiled egg plot of water partition coefficient (WlogP) *versus* topological polar surface area (TPSA) of morin *versus* reference drugs.

In case of SARS-CoV-2, morin displayed strong affinity for viral HR2 domain (PDB ID: 6LVN), viral S2 subunit (PDB ID: 6LXT), RNA binding domain of nucleocapsid phosphoprotein (PDB IDs 6VYO, 6M3M), viral spike glycoprotein (PDB ID: 6VXX), spike receptor-binding domain-ACE2 complex (PDB IDs 6LZG, 6M0J), viral RNA-dependent RNA polymerase

Table 7. Evaluation of biochemical properties of morin *versus* reference drugs calculated using SwissADME.

S. No.	Medicinal Chemistry	Morin	Baricitinib	Remdesivir	HCQ	Azithromycin
1	PAINS	0 alert	0 alert	0 alert	0 alert	0 alert
2	Brenk	0 alert	0 alert	1 alert	0 alert	0 alert
3	Lead-likeness	Yes	No 1 violation MW > 350	No 2 violations MW > 350 Rotors > 7	No 2 violations Rotors > 7 XLOGP3 > 3.5	No 2 violations MW > 350 XLOGP3 > 3.5
4	Synthetic Accessibility Score	3.25	3.07	6.33	2.82	8.91

Yes: 0 violations of rules; No: violations of rules; Rotors: no of rotatable bond; MW: molecular weight; XLOGP3: lipophilicity descriptor.

complex (PDB ID: 6M71), Nsp-9 RNA binding protein (PDB ID. 6W4B) and viral main protease 3CLpro (PDB IDs 6Y84, 6LU7, 6Y2E, 6M03) and papain- like protease PLpro (PDB ID: 6W9C), than any of the reference drugs using AutoDock 4.2.6 (Table 10). Amongst the reference drugs, baricitnib displayed strongest affinity towards viral spike protein (PDB ID: 6VYB) and human angiotensin converting enzyme2 (ACE2) receptor protein (PDB ID: 1O8A) whereas HCQ displayed greatest binding to spike protein receptor binding domain (PDB ID: 6M0J).

For the seven SARS-CoV viral proteins whose crystal structures are available in protein databank, AutoDock 4.2.6 analyses revealed that morin exhibited greatest binding affinity towards viral spike protein (PDB IDs 5WRG, 5XLR, 1WNC) and viral 3CLpro (PDB IDs 2DUC, 1Z1J) than any of the reference drugs (Table 11). Amongst the reference drugs, baricitnib displayed strongest affinity to viral main protease 3CLpro (PDB ID: 1UJ1) whereas HCQ displayed strongest binding to viral PLpro (PDB ID: 2FE8).

Out of the five MERS-CoV viral proteins whose crystal structures are available in protein databank, morin displayed strongest binding to viral PLpro (PDB IDs 4RNA, 4PT5) and viral spike glycoprotein (PDB IDs 5X5C, 5X5F, 4L3N) when compared to the three standard reference drugs (Table 12).

As mentioned above, morin was also studied with respect to its binding to three host-cell specific proteins *viz.* human ACE2 receptor (PDB ID: 1O8A), human importin-alpha1 (PDB ID: 3WPT) and poly (ADP-ribose) polymerase (PARP)-1 (PDB ID: 5DS3) as well as ILs-6, 8 and 10 (PDB IDs 1ALU, 1IL8 and 2H24, respectively). Ligands that can preferentially bind to ACE2 receptor can be thought of as promising 'preventive' agents against coronavirus infections. The binding of morin *versus* reference drugs to human ACE2 decreased in the following order: baricitinib > morin > remdesivir > HCQ (Table 10).

Inhibition of importin by ligands would interfere with viral infection and replication as well as other pathways specific to both the virus and host cell (Caly et al., 2020). In the present study, binding of morin and reference drugs to importin decreased in the order: baricitnib > morin > HCQ > remdesivir (Table 10). Interestingly, ivermectin, a repurposed antiviral drug known to inhibit importin α/β (Caly et al., 2020), was found to possess lesser affinity towards human importin-alpha1 (PDB ID: 3WPT) than morin (B.E. −5.36 kcal/mol, K_d 118.63 μM; results not shown).

Similarly, the binding of morin to poly (ADP-ribose) polymerase (PARP)-1 (PDB ID: 5DS3), a nuclear pro-inflammatory enzyme *versus* reference drugs was in the order: baricitnib > morin > HCQ > remdesivir (Table 10). The strength of binding of morin and reference drugs to IL-6 (PDB ID: 1ALU), IL-8 (PDB ID: 1IL8) and IL-10 (PDB ID: 2H24) followed the order: morin > baricitnib > HCQ > remdesivir.

3.11. Validation of docking results

Viral protein targets that elicited strong binding to morin, were redocked for further validation of results using two additional docking softwares *viz.* AutoDock vina (Tables 13–15) and iGEMDOCK v 2.1 (Tables 16–18). In case of SARS-CoV-2, AutoDock 4.2.6 results were validated for viral nucleocapsid protein (PDB ID: 6VYO, 6M3M), spike protein (PDB ID: 6VXX) and viral main protease 3CLpro (PDB ID 6Y84) using AutoDock vina (Table 13) and for nucleocapsid protein (PDB ID: 6M3M) using iGEMDOCK v 2.1 (Table 16).

In case of SARS-CoV, slight differences in B.Es and K_{ds} obtained from AutoDock 4.2.6 were observed for morin with respect to various viral target proteins using AutoDock Vina (Table 14) and iGEMDOCK v 2.1 (Table 17) whereas in case of MERS-CoV, AutoDock 4.2.6 results were validated for viral papain-like protease PLpro (PDB ID: 4RNA) using iGEMDOCK v 2.1 (Table 18).

3.12. Ligand-protein interaction visualization

Best docking poses and interacting amino acids of SARS-CoV-2, SARS-CoV and MERS-CoV target proteins with morin and the three reference drugs as well as human target proteins *viz.* ACE2, importin, PARP-1, IL-6, 8 and 10 generated using AutoDock 4.2.6 have been summarized in Supplementary Table S1, parts A–L. Similarly, best docking poses and interacting amino acids of SARS-CoV-2, SARS-CoV and MERS-CoV target proteins with morin and the three reference drugs generated using AutoDock Vina and iGEMDOCK v 2.1 have been summarized in Supplementary Table S2, parts A–L.

3.13. Molecular dynamics simulation of protein-ligand complexes

MD simulation is a tool to furnish important information about structural, conformation and fluctuation changes over time and thermodynamics of biological molecules and their complexes. Figures 7-12 depict the MD simulation analysis of morin complexed with SARS-CoV-2 main protease 3CLpro (PDB ID 6Y84) and SARS-CoV-2 papain-like protease PLpro

Figure 5. Bioavailability Radar of morin *versus* reference drugs.

(PDB ID 6W9C), respectively, using Int_mod. The receptor-ligand interaction and dynamics at atomic level of the above two complexes were also investigated using Str_mod (Supplementary Figures S3 and S4).

The stability of both protein-ligand complexes was assessed through the trajectory analysis obtained through RMSD, RMSF, radius of gyration (Rg) and fraction of native contacts (Qx) analysis over a time frame of 4000ps (4 ns).

Table 8. Bioavailability radar graphs of morin *versus* reference drugs using SwissADME.

S. No.	Ligand	LIPO	SIZE	POLAR	INSOLU	INSATU	FLEX
1	Morin	1.54	302.24 g/mol	131.36 Å^2	−3.16	0.00	1
2	Baricitinib	−0.46	371.42 g/mol	128.94 Å^2	−1.92	0.38	5
3	Remdesivir	1.91	602.58 g/mol	213.36 Å^2	−4.12	0.48	14
4	Hydroxychloroquine	3.58	335.87 g/mol	48.39 Å^2	−3.91	0.50	9
5	Azithromycin	4.02	748.98 g/mol	180.08 Å^2	−6.55	0.97	7

LIPO: Lipophilicity [−0.7< XLOGP3 < +5.0]; SIZE: Size [150 g/mol < MW < 500 g/mol]; POLAR: Polarity [20 Å2 < TPSA < 130 Å2]; INSOLU: Insolubility [0 < Log S (ESOL) < 6]; INSATU: Insaturation [0.25 < Fraction Csp3 < 1]; FLEX: Flexibility [0 < No. rotatable bonds < 9].

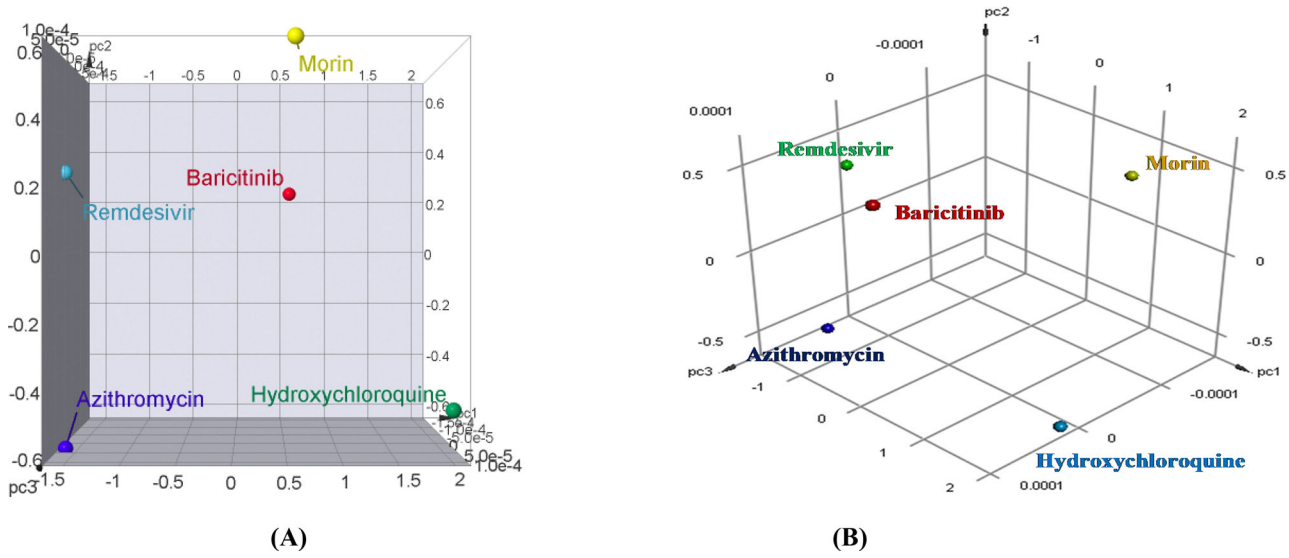

Figure 6. PCA of physicochemical properties of morin *versus* reference drugs. (A) Scatter plot and (B) 3-D point plot.

Table 9. Bravais-Pearson (linear correlation) coefficient of morin *versus* reference drugs for physicochemical properties.

r (Bravais-Pearson (linear correlation)													
Properties		1	2	3	4	5	6	7	8	9	10	11	12
% Absorbance	1		−1	−0.755	0.826	−0.774	−0.704	−0.95	−0.558	−0.836	0.977	−0.215	7.39E-05
Topological Polar Surface Area (TPSA)	2	−1		0.755	−0.826	0.774	0.705	0.95	0.558	0.836	−0.977	0.215	7.39E-05
Molecular Weight (MW)	3	−0.755	0.755		−0.342	1	0.536	0.895	0.427	0.956	−0.879	−0.478	2.16E-08
clogP	4	0.826	−0.826	−0.342		−0.361	−0.327	−0.724	−0.55	−0.462	0.714	−0.598	0.355
Heavy Atom Count (AC)	5	−0.774	0.774	1	−0.361		0.558	0.904	0.424	0.958	−0.892	−0.452	0.0125
Hydrogen bond donor (nOHNH)	6	−0.704	0.705	0.536	−0.327	0.558		0.56	0.329	0.656	−0.689	0.146	0.71
Hydrogen bond acceptor (nON)	7	−0.95	0.95	0.895	−0.724	0.904	0.56		0.547	0.914	−0.986	−0.0597	−0.155
Rotatable bond (RB)	8	−0.558	0.558	0.427	−0.55	0.424	0.329	0.547		0.644	−0.547	0.112	−0.0775
Lipinski's violation (LV)	9	−0.836	0.836	0.956	−0.462	0.958	0.656	0.914	0.644		−0.923	−0.303	0.0934
pc1	10	0.977	−0.977	−0.879	0.714	−0.892	−0.689	−0.986	−0.547	−0.923		−1.57E-08	−1.37E-08
pc2	11	−0.215	0.215	−0.478	−0.598	−0.452	0.146	−0.0597	0.112	−0.303	−1.57E-08		−2.48E-08
pc3	12	7.39E-05	7.39E-05	2.16E-08	0.355	0.0125	0.71	−0.155	−0.0775	0.0934	−1.37E-08	−2.48E-08	

RMSD is a measure of the average distance between the atoms of the overlaid structures. Often, equalized RMSD plots indicate that the system is in equilibrium. MD simulation analyses showed a satisfactory stability profile at 300 K temperature in the present study. Morin-3CLpro complex displayed very low deviation in RMSD from 0.5 to 1.5 Å throughout the 4 ns simulation (Figure 7b). Likewise morin- PLpro complex also exhibited less deviation in RMSD from 0.25 to 1.5 Å throughout the 4 ns time scale (Figure 10b). Results from RMSD analysis of both complexes suggested that the deviation in the RMSD was low; which indicated good stability and compactness of both protein-ligand complexes.

The Rg of a body is considered to be the radial distance of a point from the axis of rotation. It yields important information in the prediction of the structural activity and folding behavior of a macromolecule. The gyration radius is influenced by a change in the folding state of the protein. Rgs for morin-3CLpro (Figure 7e) and morin-PLpro (Figure 10e) complexes were found to be around 21.9 and 23.2, respectively throughout the 4 ns simulations suggesting little change in the compactness of the complex structure during the simulation thereby indicating a strong structural stability of both ligand-protein complexes. Further, to calculate the average fluctuation of all residues during simulations, RMSFs of both target proteins were plotted using morin-protein complexes. RMSF values are used to determine the atomic positional fluctuation of each amino acid *via* calculations based on their CA (Cα) atom. The comparative analysis of

Table 10. Binding energies (kcal/mol) and dissociation constants (K_d) of morin, baricitinib, remdesivir and HCQ towards selected target protein(s) of SARS-CoV-2 and human proteins using AutoDock version 4.2.6.

			Morin			Baricitinib			Remdesivir			HCQ		
S. No.	Protein	PDB ID	B.E. (kcal/mol)	Dissociation constant (K_d)	H-bond	B.E. (kcal/mol)	Dissociation constant (K_d)	H-bond	B.E. (kcal/mol)	Dissociation constant (K_d)	H-bond	B.E. (kcal/mol)	Dissociation constant (K_d)	H-bond
1	HR2 Domain	6LVN	**−5.38**	**113.69 μM**	**3**	−4.73	340.43 μM	0	−2.95	6.86 mM	1	−4.49	508.81 μM	0
2	Post fusion core of S2 subunit	6LXT	**−6.25**	**26.04 μM**	**3**	−5.01	214.17 μM	2	−5.39	111.06 μM	1	−4.63	402.22 μM	1
3	RNA binding domain of nucleocapsid phosphoprotein	6VYO	**−6.0**	**40.03 μM**	**3**	−5.54	86.75 μM	2	−4.8	305.43 μM	0	−3.49	2.76 mM	0
4	Nucleocapsid protein N-terminal RNA binding domain	6M3M	**−7.92**	**1.57 μM**	**5**	−6.4	20.46 μM	0	−6.43	19.31 μM	2	−3.63	2.18 mM	0
5	Spike ectodomain structure (open state)	6VYB	−7.2	5.29 μM	3	**−7.92**	**1.56 μM**	**1**	−1.95	37.33 mM	2	−5.98	41.36 μM	1
6	Spike glycoprotein (closed state)	6VXX	**−7.39**	**3.82 μM**	**1**	−6.71	12.11 μM	1	−2.36	18.62 mM	0	−7.05	6.76 μM	2
7	Human Angiotensin Converting Enzyme (Native)	1O8A	−6.99	7.55 μM	5	**−7.28**	**4.59 μM**	**2**	−6.66	13.11 μM	0	−5.75	60.73 μM	1
8	Closed dimer of human importin-alpha1 (Rch1)	3WPT	−5.36	118.63 μM	2	**−5.44**	**103.13 μM**	**1**	−3.25	4.12 mM	2	−4.21	825.15 μM	0
9	Poly [ADP-ribose] polymerase 1	5DS3	−6.94	8.12 μM	3	**−8.64**	**465.15 nM**	**2**	−4.11	973.43 μM	0	−5.4	109.97 μM	1
10	Human Interleukin-6 (IL-6)	1ALU	**−6.57**	**15.18 μM**	**4**	−4.43	569.32 μM	0	—	—	—	−2.64	11.56 mM	1
11	human Interleukin-10 (IL-10)	2H24	**−5.98**	**41.45 μM**	**1**	−4.93	242.57 μM	2	−1.78	49.65 mM	0	−3.71	1.91 mM	0
12	Human Interleukin-8	1IL8	**−6.07**	**35.26 μM**	**4**	−5.66	71.14 μM	0	—	—	—	−3.91	1.37 mM	0
13	Spike receptor-binding domain complexed with its receptor ACE2	6LZG	**−6.9**	**8.78 μM**	**4**	−6.76	11.16 μM	0	−6.43	19.46 μM	1	−6.22	27.56 μM	1
14	Spike receptor binding domain bound with ACE2	6M0J	**−6.81**	**10.23 μM**	**2**	−6.21	27.84 μM	0	−5.35	120.56 μM	1	−6.96	7.94 μM	2
15	RNA-dependent RNA polymerase complex with cofactors	6M71	**−6.54**	**16.09 μM**	**4**	−6.22	27.43 μM	4	−4.31	687.27 μM	1	−3.46	2.89 mM	0
16	Nsp-9 RNA binding protein	6W4B	**−6.49**	**17.47 μM**	**2**	−6.16	30.75 μM	1	−2.31	20.35 mM	1	−4.03	1.12 mM	0
17	Main protease (3CLpro) with unliganded active site	6Y84	**−7.7**	**2.27 μM**	**2**	−6.43	19.45 μM	1	−7.22	5.12 μM	1	−5.62	75.35 μM	1
18	Main protease (3CLpro) in complex with an inhibitor N3	6LU7	**−6.52**	**16.69 μM**	**3**	−4.8	304.41 μM	0	−0.56	388.09 mM	0	−4.24	785.19 μM	1
19	Free enzyme of Main protease (3CLpro)	6Y2E	**−6.68**	**12.75 μM**	**4**	−5.29	133.67 μM	1	—	—	—	−3.57	2.41 mM	1
20	Main protease (3CLpro) in apo form	6M03	**−5.24**	**145.16 μM**	**2**	−4.7	360.76 μM	1	—	—	—	−3.17	4.73 mM	1
21	Papain-like protease (PLpro)	6W9C	**−7.64**	**2.51 μM**	**1**	−7.36	4.03 μM	3	−5.3	129.61 μM	0	−5.89	47.87 μM	0

Bold values indicate good binding energies.
'—' indicates no binding detected.

Table 11. Binding energies (kcal/mol) and dissociation constants (K_d) of morin, baricitinib, remdesivir and HCQ towards selected target protein(s) of SARS-CoV using AutoDock version 4.2.6.

			Morin			Baricitinib			Remdesivir			HCQ		
S. No.	Protein	PDB ID	B.E. (kcal/mol)	Dissociation constant (K_d)	H-bond	B.E. (kcal/mol)	Dissociation constant (K_d)	H-bond	B.E. (kcal/mol)	Dissociation constant (K_d)	H-bond	B.E. (kcal/mol)	Dissociation constant (K_d)	H-bond
1	Main protease (3CLpro)	2DUC	**−8.47**	**622.2 nM**	**4**	−8.26	880.74 nM	3	−3.68	2.0 mM	0	−4.72	345.05 μM	1
2	Main Protease (3CLpro)	1UJ1	−8.77	372.91 nM	4	**−9.13**	**204.53 nM**	**3**	−2.73	9.95 mM	2	−5.13	174.53 μM	1
3	Main Protease (3CLpro) C145A mutant	1Z1J	**−8.65**	**453.68 nM**	**4**	−7.77	2.03 μM	2	−1.92	39.01 mM	2	−5.35	119.42 μM	1
4	Papain-like protease (PLpro): structure of a viral deubiquitinating enzyme	2FE8	**−5.54**	**87.45 μM**	**2**	−4.38	617.24 μM	0	−4.18	868.58 μM	3	−5.58	81.55 μM	2
5	Spike glycoprotein	5WRG	**−8.0**	**1.36 μM**	**5**	−6.42	19.53 μM	0	—	—	—	−5.58	81.46 μM	1
6	Spike glycoprotein	5XLR	**−5.34**	**122.15 μM**	**2**	−4.45	542.97 μM	1	—	—	—	−4.35	649.02 μM	0
7	Spike protein fusion core	1WNC	**−7.35**	**4.1 μM**	**4**	−6.55	15.78 μM	1	−3.81	1.61 mM	4	−5.34	121.88 μM	1

Bold values indicate good binding energies.
'—' indicates no binding detected.

Table 12. Binding energies (kcal/mol) and dissociation constants (K_d) of morin, baricitinib, remdesivir and HCQ towards selected target protein(s) of MERS-CoV using AutoDock version 4.2.6.

			Morin			Baricitinib			Remdesivir			HCQ		
S. No.	Protein	PDB ID	B.E. (kcal/mol)	Dissociation constant (K_d)	H-bond	B.E. (kcal/mol)	Dissociation constant (K_d)	H-bond	B.E. (kcal/mol)	Dissociation constant (K_d)	H-bond	B.E. (kcal/mol)	Dissociation constant (K_d)	H-bond
1	Papain-like protease (PLpro)	4RNA	**−5.57**	**83.31 μM**	**2**	−4.9	254.97 μM	0	−1.41	91.86 mM	0	−4.19	849.18 μM	0
2	Papain-like protease (PLpro)	4PT5	**−5.08**	**188.91 μM**	**1**	−4.38	618.96 μM	0	−0.73	290.39 mM	1	−4.12	956.12 μM	0
3	Prefusion structure of spike glycoprotein, conformation 1	5X5C	**−6.68**	**12.64 μM**	**1**	−5.69	67.48 μM	1	−3.62	2.21 mM	1	−5.3	129.91 μM	0
4	Prefusion structure of spike glycoprotein, conformation 2	5X5F	**−6.26**	**25.73 μM**	**1**	−5.51	92.04 μM	0	−3.87	1.46 mM	1	−5.19	158.05 μM	0
5	Receptor-binding domain	4L3N	**−7.8**	**1.92 μM**	**5**	−5.74	61.87 μM	2	−4.13	942.43 μM	1	−4.39	604.87 μM	1

Bold values indicate good binding energies.

Table 13. Binding energies (kcal/mol) and dissociation constants (K_d) of morin, baricitinib, remdesivir and HCQ towards selected target protein(s) of SARS-CoV-2 using AutoDock Vina.

			Morin		Baricitinib		Remdesivir		HCQ	
S. No.	Protein	PDB ID	B.E. (kcal/mol)	Dissociation constant (K_d)	B.E. (kcal/mol)	Dissociation constant (K_d)	B.E. (kcal/mol)	Dissociation constant (K_d)	B.E. (kcal/mol)	Dissociation constant (K_d)
1	HR2 Domain	6LVN	−6.6	13.57 μM	−5.4	102.3 μM	**−8.2**	**959.88 nM**	−5.4	102.41 μM
2	Post fusion core of S2 subunit	6LXT	−7.6	2.51 μM	−7.0	6.67 μM	**−9.1**	**213.45 nM**	−6.7	10.64 μM
3	RNA binding domain of nucleocapsid phosphoprotein	6VYO	**−8.6**	**487.1 nM**	−7.3	4.12 μM	−8.3	916.21 nM	−6.8	9.26 μM
4	Nucleocapsid protein N-terminal RNA binding domain	6M3M	**−8.9**	**295.92 nM**	−8.8	334.17 nM	−8.6	453.68 nM	−6.2	24.67 μM
5	Spike glycoprotein (closed state)	6VXX	**−8.5**	**570.25 nM**	−8.4	642.92 nM	−8.2	855.53 nM	−6.6	14.14 μM
6	Spike receptor-binding domain complexed with its receptor ACE2	6LZG	−9.4	128.98 nM	−7.6	2.96 μM	**−10.3**	**25.67 nM**	−6.5	15.36 μM
7	RNA-dependent RNA polymerase complex with cofactors	6M71	−7.9	1.56 μM	−7.3	4.1 μM	**−8.8**	**314.24 nM**	−6.3	23.21 μM
8	Nsp-9 RNA binding protein	6W4B	−7.1	6.05 μM	−6.3	23.21 μM	**−7.6**	**2.29 μM**	−5.6	83.92 μM
9	Main protease (3CLpro)with unliganded active site	6Y84	**−9.7**	**90.74 nM**	−8.3	734.86 nM	−9.6	103.1 nM	−7.4	3.22 μM
10	Main protease (3CLpro) in complex with an inhibitor N3	6LU7	−8.2	855.52 nM	−.6.6	13.45 μM	**−9.4**	**129.59 nM**	−5.7	58.49 μM
11	Free enzyme of Main protease (3CLpro)	6Y2E	−7.8	1.57 μM	−7.0	7.42 μM	**−8.5**	**568.67 nM**	−6.2	23.89 μM
12	Main protease (3CLpro) in apo form	6M03	−7.6	2.81 μM	−6.7	11.83 μM	**−9.0**	**238.74 nM**	−5.9	40.63 μM
13	Papain-like protease (PLpro)	6W9C	−8.1	1.36 μM	−8.4	641.98 nM	**−9.5**	**104.4 nM**	−7.1	6.05 μM

Bold values indicate good binding energies.

Table 16. Total energies (kcal/mol), van der Waals, hydrogen bonding and electrostatic energies of morin *versus* reference drugs towards selected target protein(s) of SARS-CoV-2 using iGEMDOCKv2.1.

			Morin				Baricitinib				Remdesivir				HCQ			
S. No.	Protein	PDB ID	T.E. (kcal/mol)	vDW	HB	EI	T.E. (kcal/mol)	vDW	HB	EI	T.E. (kcal/mol)	vDW	HB	EI	T.E. (kcal/mol)	vDW	HB	EI
1	HR2 Domain	6LVN	−76.50	−61.93	−14.57	0	−76.29	−52.79	−23.49	0	**−94.19**	**−75.33**	**−18.85**	**0**	−69.67	−69.67	0	0
2	Post fusion core of S2 subunit	6LXT	−94.40	−71.17	−23.23	0	−90.63	−72.93	−17.70	0	**−104.18**	**−79.48**	**−24.70**	**0**	−78.49	−74.99	−3.5	0
3	RNA binding domain of nucleocapsid phosphoprotein	6VYO	−100.14	−77.82	−22.31	0	−99.81	−74.11	−25.70	0	**−101.23**	**−79.30**	**−21.92**	**0**	−84.16	−76.31	−7.84	0
4	Nucleocapsid protein N-terminal RNA binding domain	6M3M	**−118.31**	**−92.57**	**−25.74**	**0**	−96.54	−77.13	−19.40	0	−110.92	−79.71	−31.21	0	−83.65	−78.72	−4.93	0
5	Spike glycoprotein (closed state)	6VXX	−110.22	−89.09	−21.12	0	−99.83	−68.61	−31.21	0	**−110.59**	**−87.91**	**−22.68**	**0**	−83.01	−76.67	−6.34	0
6	Spike receptor-binding domain complexed with its receptor ACE2	6LZG	**−106.50**	**−84.93**	**−21.57**	**0**	−105.1	−85.11	19.98	0	−96.28	−73.57	−22.71	0	−88.76	−72.26	−16.5	0
7	RNA-dependent RNA polymerase complex with cofactors	6M71	−94.55	−66.16	−28.39	0	−94.22	−75.10	−19.11	0	**−114.92**	**−79.37**	**−35.55**	**0**	−89.94	−77.35	−12.59	0
8	Nsp-9 RNA binding protein	6W4B	−94.81	−78.21	−16.59	0	−86.57	−74.52	−12.04	0	**−96.08**	**−77.67**	**−18.41**	**0**	−64.87	−58.87	−6	0
9	Main protease (3CLpro)with unliganded active site	6Y84	−107.17	−73.85	−33.32	0	−95.33	−71.74	−23.58	0	**−108.29**	**−85.80**	**−22.49**	**0**	−77.65	−70.79	−6.85	0
10	Main protease (3CLpro) in complex with an inhibitor N3	6LU7	**−108.63**	**−76.03**	**−32.60**	**0**	−82.75	−59.83	−22.91	0	−100.20	−72.05	−28.15	0	−66.91	−55.61	−11.29	0
11	Free enzyme of Main protease (3CLpro)	6Y2E	−110.09	−69.08	−41.00	0	−93.44	−78.53	14.90	0	**−115.97**	**−88.06**	**−27.90**	**0**	−78.094	−68.45	−9.64	0
12	Main protease (3CLpro) in apo form	6MO3	−103.48	−63.67	−39.80	0	−99.25	−53.04	−46.20	0	**−114.64**	**−87.34**	**−27.29**	**0**	−78.09	−65.64	−12.44	0
13	Papain-like protease (PLpro)	6W9C	−100.52	−80.26	−20.26	0	−100.15	−76.79	−23.35	0	**−114.96**	**−94.36**	**−20.59**	**0**	−80.98	−80.98	0	0

Bold values indicate good binding energies.
vdW: van der Waals energy; HB: hydrogen bonding energy; EI: electrostatic energy.

Table 14. Binding energies (kcal/mol) and dissociation constants (K_d) of morin *versus* reference drugs towards selected target protein(s) of SARS-CoV using AutoDock Vina.

			Morin		Baricitinib		Remdesivir		Hydroxycholoroquine	
S. No.	Protein	PDB ID	B.E. (kcal/mol)	Dissociation constant (K_d)	B.E. (kcal/mol)	Dissociation constant (K_d)	B.E. (kcal/mol)	Dissociation constant (K_d)	B.E. (kcal/mol)	Dissociation constant (K_d)
1	Main protease (3CLpro)	2DUC	−8.8	325.96 nM	−8.8	322.91 nM	**−9.6**	**94.36 nM**	−6.5	14.87 μM
2	Spike glycoprotein	5WRG	−8.3	820.05 nM	−8.7	372.90 nM	**−9.3**	**136.01 nM**	−6.7	12.26 μM
3	Spike glycoprotein	5XLR	−8.2	959.88 nM	−8.4	625.25 nM	**−9.7**	**70.23 nM**	−6.9	8.73 μM
4	Spike protein fusion core	1WNC	−8.3	821.08 nM	−6.7	12.89 μM	**−9.1**	**212.78 nM**	−6.3	21.53 μM

Bold values indicate good binding energies.

Table 15. Binding energies (kcal/mol) and dissociation constants (K_d) of morin *versus* reference drugs towards selected target protein(s) of MERS-CoV using AutoDock Vina.

			Morin		Baricitinib		Remdesivir		HCQ	
S. No.	Protein	PDB ID	B.E. (kcal/mol)	Dissociation constant (K_d)	B.E. (kcal/mol)	Dissociation constant (K_d)	B.E. (kcal/mol)	Dissociation constant (K_d)	B.E. (kcal/mol)	Dissociation constant (K_d)
1	Papain-like protease (PLpro)	4RNA	−7.5	2.75 μM	−6.9	7.94 μM	**−7.7**	**2.18 μM**	−5.7	84.94 μM
2	Papain-like protease (PLpro)	4PT5	−7.1	5.78 μM	−6.1	3.99 μM	**−7.5**	**2.90 μM**	−6.0	34.22 μM
3	Prefusion structure of spike glycoprotein, conformation 1	5X5C	−9.5	100.36 nM	−8.5	635.11 nM	**−9.8**	**67.23 nM**	−7.0	7.42 μM
4	Prefusion structure of spike glycoprotein, conformation 2	5X5F	−8.8	334.17 nM	−8.6	485.46 nM	**10.0**	**40.9 nM**	−7.1	5.96 μM
5	Receptor-binding domain	4L3N	−7.4	3.25 μM	−6.7	12.26 μM	**−8.7**	**371.92 nM**	−5.8	49.23 μM

Bold values indicate good binding energies.

Table 17. Total energies (kcal/mol), van der Waals, hydrogen bonding and electrostatic energies of morin *versus* reference drugs towards selected target protein(s) of SARS-CoV using iGEMDOCKv2.1.

			Morin				Baricitinib				Remdesivir				HCQ			
S. No.	Protein	PDB ID	T.E. (kcal/mol)	vDW	HB	EI	T.E. (kcal/mol)	vDW	HB	EI	T.E. (kcal/mol)	vDW	HB	EI	T.E. (kcal/mol)	vDW	HB	EI
1	Main protease (3CLpro)	2DUC	**−109.62**	**−82.94**	**−26.67**	**0**	−100.22	−86.60	−13.61	0	**−105.32**	**−79.01**	**−26.31**	**0**	−77.72	−70.68	−7.03	0
2	Spike glycoprotein	5WRG	−92.39	−56.49	−35.90	0	−102.54	−64.49	−38.04	0	**−113.33**	**−71.25**	**−42.08**	**0**	−82.31	−74.59	−7.71	0
3	Spike glycoprotein	5XLR	**−108.76**	**−81.32**	**−27.44**	**0**	−94.67	−68.22	−26.45	0	−104.79	−84.16	−20.62	0	−79.08	−67.34	−11.74	0
4	Spike protein fusion core	1WNC	−95.24	−83.46	−11.77	0	−90.36	−64.04	−26.32	0	−97.83	−73.54	−24.28	0	−73.90	−67.90	−6	0

Bold values indicate good binding energies.
vdW: van der Waals energy; HB: hydrogen bonding energy; EI: electrostatic energy.

RMSF trajectories indicated that all amino acid residues in the complex model of morin-3CLpro fluctuated between 0 to 15 Å (Figure 7g), while in case of morin-PLpro complex, RMSF value was found to fluctuate between 0 to 20 Å (Figure 10g).

In the folding process, certain cases of non-native interactions are considered to be irrelevant and there are certain simulations as well as folding models which support that only native contacts are energetically favorable. Therefore, Fraction of Native Contacts Q (x) helps in capturing the transition states remarkably well for all proteins along with a folding free energy barrier. In the present study, the Qx value was found to be larger than 95% in both complexes, thus indicating the relative flexibility and increased stability of the both complexes throughout the simulation period (Figures 7f and 10f). B-factor, also termed as the temperature factor, is a factor similar to RMSF and is used to describe the attenuation of x-ray scattering resulting due to thermal motion. B-factors of both complexes fluctuated around 2000 and 4000, respectively, which indicated thermal stability of both the complexes (Figures 7h,i and 10h,i).

PCA is used to detect nature of conformational differences, while magnitude of pairwise cross-correlation coefficients indicate system's atomic variations associated with each other. As is evident from Figures 8 and 11, the correlated residues are blue colored whereas, non-correlated residues are in red. The light pink and light blue lines represent pairwise residues with higher correlated coefficient (>0.8) and with higher non-correlated coefficient (< -0.4). The schematic representation of secondary structures are present on the top and right margins of dynamical residue cross-correlation map as black helices, grey strands and white loops.

MM/PB(GB)SA result analysis mainly comprises of electrostatic energy (ELE), van der Waals contribution (VDW), total gas phase energy (GAS), non-polar and polar contributions to solvation (PBSOL/GBSOL). The finally recorded binding free energy (deltaPB/deltaGB) is calculated from PBTOT/GBTOT and entropy (TS) as shown in Figures 9(a) and 12(a). Further, hydrogen bond analysis includes the hydrogen bond acceptor and donor atoms, average distance (Avg Dist), angle (Avg Ang), and proportion (Frac) as shown in Figures 9(b,c) and 12(b,c). Moreover, the results of decompose

Table 18. Total energies (kcal/mol), van der Waals, hydrogen bonding and electrostatic energies of morin *versus* reference drugs towards selected target protein(s) of MERS-CoV using iGEMDOCKv2.1.

S. No.	Protein	PDB ID	Morin				Baricitinib				Remdesivir				HCQ			
			T.E. (kcal/mol)	vDW	HB	EI	T.E. (kcal/mol)	vDW	HB	EI	T.E. (kcal/mol)	vDW	HB	EI	T.E. (kcal/mol)	vDW	HB	EI
1	Papain-like protease (PLpro)	4RNA	**−100.86**	**−82.30**	**−18.56**	**0**	−92.36	−80.85	−11.51	0	−97.55	−80.23	−17.32	0	−76.58	−66.71	−9.87	0
2	Papain-like protease (PLpro)	4PT5	**−99.17**	**−81.47**	**−17.70**	**0**	−83.06	−63.84	−19.21	0	−93.52	−57.19	−36.32	0	−74.74	−69.82	−4.92	0
3	Prefusion structure of spike glycoprotein, conformation 1	5X5C	**−114.82**	**−89.36**	**−25.46**	**0**	−94.40	−75.92	−18.48	0	−105.17	−87.42	−17.74	0	−80.59	−68.67	−11.91	0
4	Prefusion structure of spike glycoprotein, conformation 2	5X5F	−103.76	−80.14	−23.62	0	−96.21	−86.39	−9.82	0	**−109.04**	**−83.46**	**−25.58**	**0**	−75.29	−74.79	−0.49	0
5	Receptor-binding domain	4L3N	−98.80	−73.80	−25.00	0	−94.20	−72.04	−22.15	0	**−104.94**	**−86.54**	**−18.40**	**0**	−85.10	−66.15	−18.94	0

Bold values indicate good binding energies.
vdW: van der Waals energy; HB: hydrogen bonding energy; EI: electrostatic energy.

comprises of electrostatic energy which is calculated by the MM force field (TELE), van der Waals contribution from MM (TVDW), sum of non-polar and polar contributions to solvation (TGBSOL), total gas phase energy (TGAS) and final estimation of binding free energy from TGBTOT. Depending on the 'TGBTOT' energy, the residues with contribution are ranked into top 10 decompose calculations which are arranged from top to bottom in heatmap (Figures 9d and 12d).

4. Discussion

Flavonoids are polyphenolic compounds classified into flavonols, flavones, flavanones, isoflavones, catechins, anthocyanidins and chalcones according to their chemical structures. They are naturally occurring and more than 8,000 flavonoids have been described from different plant sources. Flavonoids have been reported to possess antiviral, anti-allergic, antiplatelet, antitumor, antioxidant and anti-inflammatory activities and interest in these compounds has been increasing since they are presumed to be beneficial to human health. The anti-inflammatory and antioxidant properties of flavonoids make them likely candidates for evaluation in pulmonary diseases (Bravo, 1998; Caltagirone et al., 1997; Ranelletti et al., 1992; Yoshida et al., 1990). Additionally, flavonoids protect cells by inhibiting enzymes and proteins involved in cell proliferation and apoptosis (Lee & Yoo, 2013).

Lung diseases involve acute or chronic inflammation that culminates in a repair process which is highly associated with a decrement in lung function. Flavonoids have become a constant fixture in folk medicine since time immemorial and several studies have proven their anti-inflammatory and antioxidant nature (Lim et al., 2013). Therefore, flavonoids may be beneficial in inhibiting or reducing the progression of pulmonary disease in patients with chronic obstructive pulmonary disease (COPD), lung cancer, acute respiratory distress syndrome (ARDS) and asthma. Owing to their anti-inflammatory nature, flavonoids are expected to have a modulatory effect in inflammatory diseases like ARDS, SARS COPD and asthma. However, most of the existing studies till date have been done in experimental models (Chen et al., 2013; Tseng et al., 2012).

The anti-inflammatory activity of flavonol morin is attributed to its inhibition of enzyme lipoxygenase and cyclooxygenase (Cao et al., 1997; Cazarolli et al., 2008; O'Leary et al., 2004; Yoon & Baek, 2005). Morin and its analogs have also been found to inhibit urease, a nickel containing metalloenzyme (Kataria & Khatkar, 2019). Morin has also been found to inhibit poly (ADP-ribose) polymerase (PARP)-1, a nuclear pro-inflammatory enzyme involved in the signal transduction pathway of COPD, thus making it a potential nutraceutical agent for COPD patients (Weseler et al., 2009). This is in agreement with the present study in which morin *versus* reference antiviral drugs displayed potent binding to human (PARP)-1 (PDB ID: 5DS3) (Table 10). Morin has also been found to suppress the LPS-induced release of pro-inflammatory cytokines TNF-α, IL-6, IL-8 and IL-10 from leukocytes in COPD patients (Weseler et al., 2009). Interestingly, this was

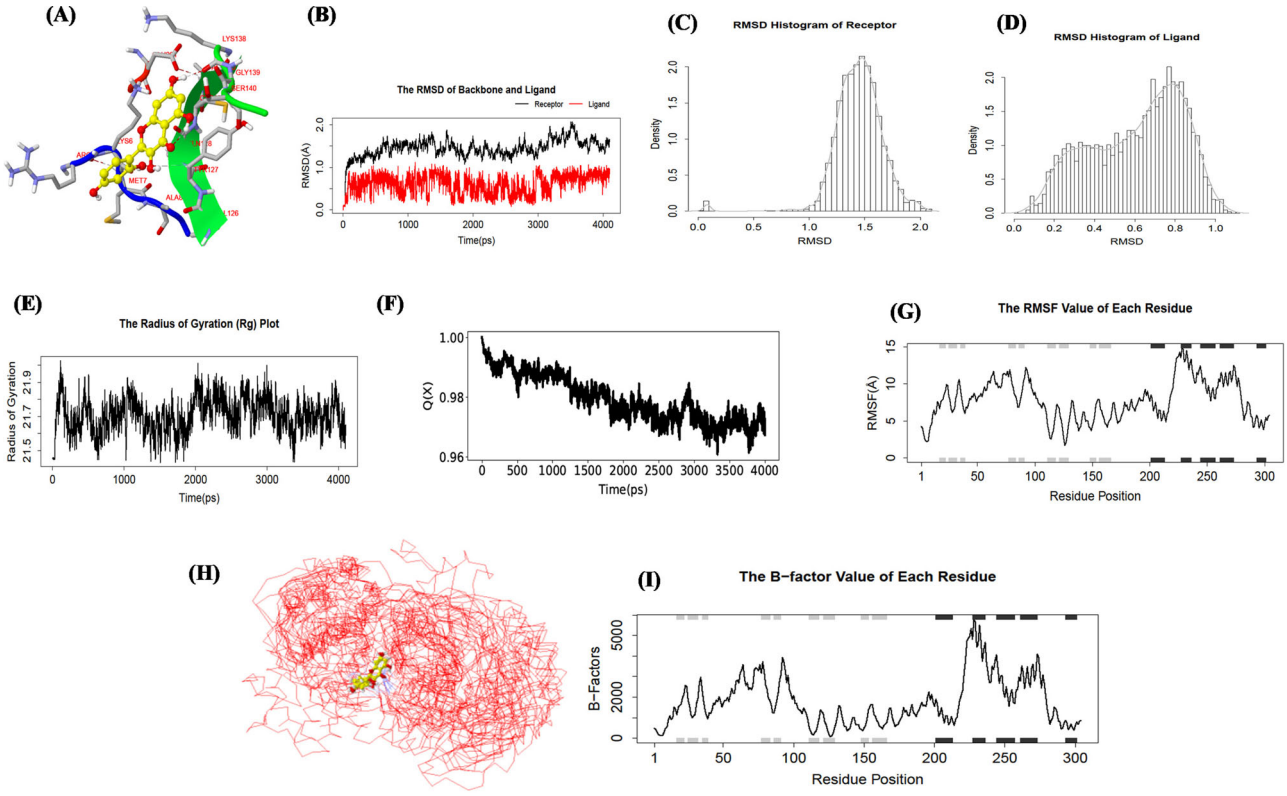

Figure 7. MD Simulation of morin complexed with SARS-CoV-2 main protease 3CLpro (PDB ID: 6Y84). (A) Ligand-protein conformation (B) RMSD of receptor and ligand (morin) (C) RMSD histogram of receptor (D) RMSD histogram of ligand (morin) (E) Radius of gyration, Rg value (F) Fraction of native contacts analysis of SARS-CoV-2 CLpro with morin over a time frame of 4000ps (4 ns) (G) RMSF value of each residue (H) B-factor value (changing from blue to red with increase in value) and (I) B-factor analysis of defined complex (Int_mod).

also found in agreement with the obtained results of the present study depicted in Table 10.

Additionally, morin has been found to be effective in asthma models both in the early and late response. Morin is also known to inhibit HIV-l protease (Brinkworth et al., 1992); this is in agreement with the docking results obtained in the present study with morin against SARS-CoV-2, SARS-CoV and MERS-CoV proteases (Tables 10–12). Morin is also known to act as an inhibitor of protein kinase C (Ferriola et al., 1989); this also is in agreement with the obtained BAS values for morin in the present study (Table 2), aldose reductase (Varma et al., 1986), glutathione reductase (Elliott et al., 1992), histamine release from basophils (Middleton & Drzewiecki, 1982) and iodothyronine deiodinase (Auf'mkolk et al., 1986; Cody et al., 1986; Koehrle et al., 1989). A meta-analysis of seven studies has revealed that COPD patients have a significantly higher risk of developing severe COVID-19 complications (https://www.medicalnewstoday.com/articles/covid-19-and-copd#danger). Therefore, it would be worthwhile to evaluate the efficacy of morin in COPD patients harboring COVID-19 infection (Jih, 2005; Rubenfeld, 2003).

Inflammation is closely related to disease severity in COVID-19 (Rahmati & Moosavi, 2020). Hyper-inflammation induced by massive release of cytokines/chemokines, called as cytokine storm, leads to serious complications like fatal pneumonia and ARDS in COVID-19 (Huang et al., 2020; Zhang et al., 2020). The understanding of the cytokine storm mechanism(s) and its profile are crucial to developing effective therapeutic interventions in COVID-19 (Zumla et al., 2020). A current report has presented different cytokine profiles in patients with severe COVID-19 (Gong et al., 2020). To this effect, cytokine storm blockers and immune-host modulators are currently being applied in severely ill COVID-19 patients to cope with the overwhelming inflammation.

As SARS-CoV-2 uses the ACE2 receptor expressed on human airway epithelia and lung parenchyma cells for host cell entry, morin was investigated for its binding kinetics to the human ACE2 receptor. Results of molecular docking analysis using AutoDock v4.2.6 showed that morin *versus* reference drugs displayed good binding affinities with ACE2 receptor in the following order: baricitinib > morin > remdesivir > HCQ (Table 10). Morin was also evaluated for its ability to bind importin alpha-1. In this study, binding affinity of morin *versus* reference drugs to importin was found to be in the order: baricitnib > morin > HCQ > remdesivir (Table 10). The transport of proteins between the cytoplasm and nucleus which is mediated by the importin superfamily of proteins is essential to many cellular processes, such as differentiation and development and is also critical to induction of viral diseases and oncogenesis (Caly et al., 2020). Importin (IMP) $\alpha/\beta 1$ is a heterodimeric protein responsible for nuclear import of viral proteins *viz*. non-structural proteins (NSPs) of many RNA viruses (Wagstaff et al., 2011) that replicate exclusively in the cytoplasm like HIV-1 (Wagstaff et al., 2012), dengue virus DENV 1-4 (Tay et al., 2013), West Nile Virus (Yang

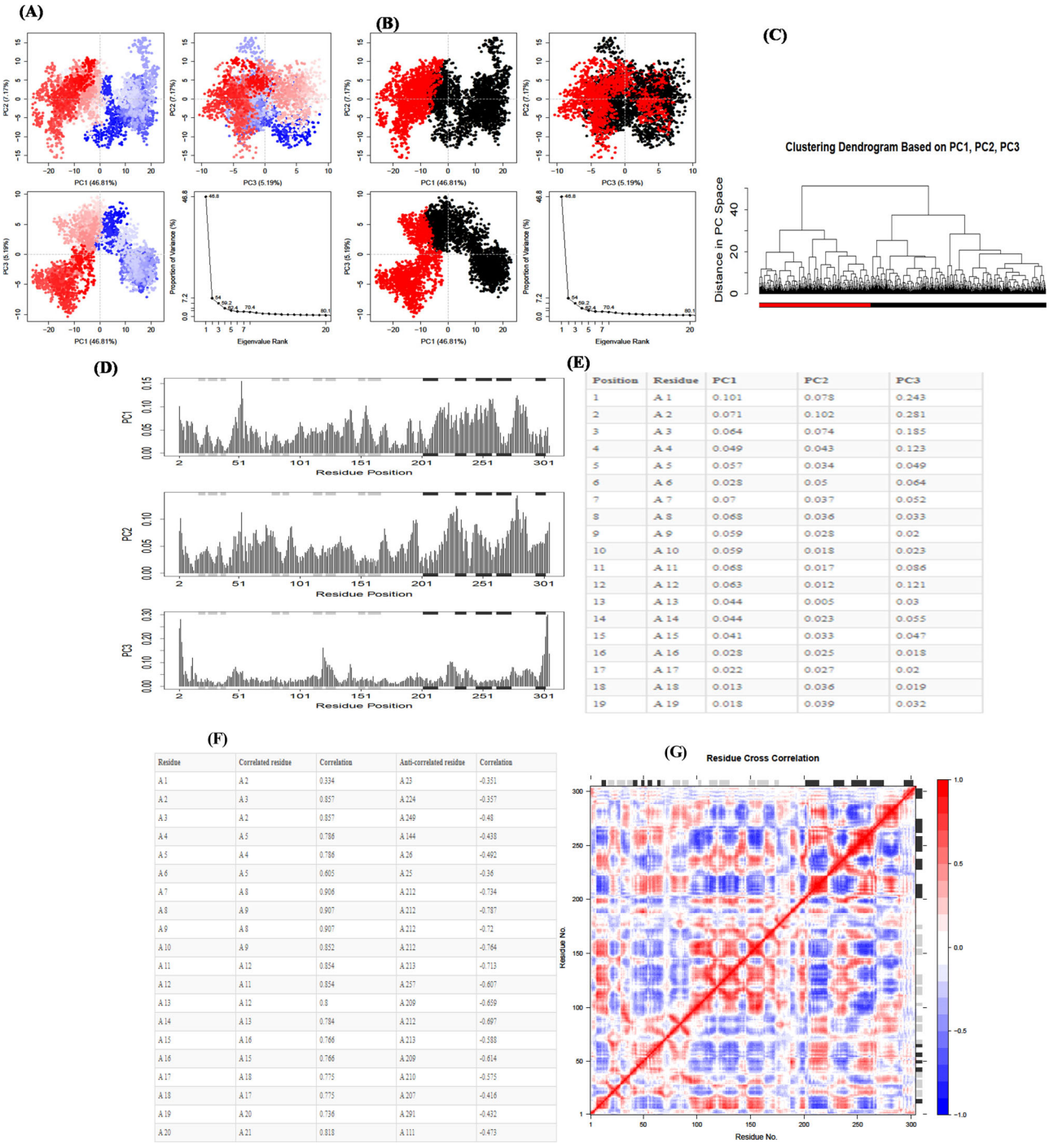

Position	Residue	PC1	PC2	PC3
1	A 1	0.101	0.078	0.243
2	A 2	0.071	0.102	0.281
3	A 3	0.064	0.074	0.185
4	A 4	0.049	0.043	0.123
5	A 5	0.057	0.034	0.049
6	A 6	0.028	0.05	0.064
7	A 7	0.07	0.037	0.052
8	A 8	0.068	0.036	0.033
9	A 9	0.059	0.028	0.02
10	A 10	0.059	0.018	0.023
11	A 11	0.068	0.017	0.086
12	A 12	0.063	0.012	0.121
13	A 13	0.044	0.005	0.03
14	A 14	0.044	0.023	0.055
15	A 15	0.041	0.033	0.047
16	A 16	0.028	0.025	0.018
17	A 17	0.022	0.027	0.02
18	A 18	0.013	0.036	0.019
19	A 19	0.018	0.039	0.032

Residue	Correlated residue	Correlation	Anti-correlated residue	Correlation
A 1	A 2	0.334	A 23	-0.351
A 2	A 3	0.857	A 224	-0.357
A 3	A 2	0.857	A 249	-0.48
A 4	A 5	0.786	A 144	-0.438
A 5	A 4	0.786	A 26	-0.492
A 6	A 5	0.605	A 25	-0.36
A 7	A 8	0.906	A 212	-0.734
A 8	A 9	0.907	A 212	-0.787
A 9	A 8	0.907	A 212	-0.72
A 10	A 9	0.852	A 212	-0.764
A 11	A 12	0.854	A 213	-0.713
A 12	A 11	0.854	A 257	-0.607
A 13	A 12	0.8	A 209	-0.659
A 14	A 13	0.784	A 212	-0.697
A 15	A 16	0.766	A 213	-0.588
A 16	A 15	0.766	A 209	-0.614
A 17	A 18	0.775	A 210	-0.575
A 18	A 17	0.775	A 207	-0.416
A 19	A 20	0.736	A 291	-0.432
A 20	A 21	0.818	A 111	-0.473

Figure 8. PCA of SARS-CoV-2 3CLpro (PDB ID: 6Y84) complexed with morin (A) PCA results for Trajectory (B) Simple clustering in PC subspace (C) Clustering dendrogram based on PC1, PC2 and PC3 (D) Residue-wise loadings for PC1, PC2 and PC3 (E) Table data showing residue-wise loadings for PC1, PC2 and PC3 and residue number at each position (F) Table showing pair-wise cross-correlation coefficients; higher correlated coefficient value is >0.8 and higher anti-correlated coefficient value is < -0.4 (G) Dynamical Residue Cross-correlation Map; the correlated residues are in blue, anti-correlated residues are in red; the pairwise residues with higher correlated coefficient (>0.8) and with higher anti-correlated coefficient (< -0.4) are linked with light pink and light blue (Int_mod).

et al., 2020b), Venezuelan equine encephalitis virus (VEEV) (Lundberg et al., 2013) and influenza (Götz et al., 2016) during infection (Caly et al., 2012; Jans et al., 2019). In case of DENV, a major part of NSP 5 has been found to be localized in the host cell nucleus during certain parts of the virus infectious life cycle, despite its critical role in viral replication, which occurs in the cytoplasm and that mutation of critical residues in the Impα/β1-recognized nuclear-localization signal (NLS) severely inhibits virus production (Pryor et al., 2007). Similarly, MERS-CoV NSP1 has been found to be localized both in the cytoplasm and the nuclei of host cells (Lokugamage et al., 2015), unlike SARS-CoV NSP1, which is a cytoplasmic protein (Kamitani et al., 2006). Interestingly, MERS-CoV NSP1 selectively inhibits translation and induces degradation of host-specific mRNAs (Lokugamage et al., 2015; Nakagawa et al., 2016). NSPs 3 and 5 of SARS-CoV-2

(A)

ELE	VDW	GAS	PBSOL	PBTOT	GBSOL	GBTOT	TS	deltaPB	deltaGB
-6.76	-27.35	-34.11	15.19	-18.92	12.52	-21.59	17.29	-1.63	-4.30

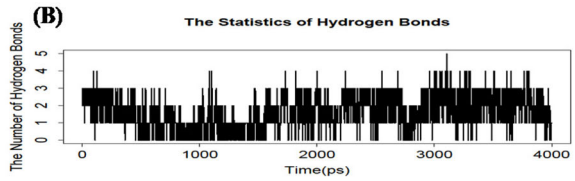

(C)

Acceptor	DonorH	Donor	Frames	Frac	AvgDist	AvgAng
A 138 : GLY@N	0 : UNN@H8	0 : UNN@O6	1	0.0002	3.4783	145.0972
A 139 : SER@N	0 : UNN@H7	0 : UNN@O5	1	0.0002	3.4728	134.3637
A 127 : GLN@N	0 : UNN@H6	0 : UNN@O4	1	0.0002	3.4681	130.2388
A 138 : GLY@O	0 : UNN@H7	0 : UNN@O5	1	0.0002	3.4320	120.6823
A 124 : GLY@N	0 : UNN@H7	0 : UNN@O5	1	0.0002	3.4159	129.0563
A 5 : LYS@NZ	0 : UNN@H8	0 : UNN@O6	1	0.0002	3.4067	123.8850
A 123 : SER@OG	0 : UNN@H7	0 : UNN@O5	1	0.0002	3.2257	120.0384
A 126 : TYR@OH	0 : UNN@H7	0 : UNN@O5	2	0.0005	3.4031	123.6563
A 125 : VAL@N	0 : UNN@H5	0 : UNN@O3	2	0.0005	3.3758	133.8195
A 1 : SER@OG	0 : UNN@H9	0 : UNN@O7	2	0.0005	3.1656	132.0657
A 125 : VAL@O	0 : UNN@H7	0 : UNN@O5	2	0.0005	3.0971	129.9954
A 126 : TYR@OH	0 : UNN@H8	0 : UNN@O6	3	0.0007	3.3376	132.4164
A 127 : GLN@O	0 : UNN@H5	0 : UNN@O3	3	0.0007	3.3081	129.6542
A 290 : GLU@OE1	0 : UNN@H7	0 : UNN@O5	3	0.0007	2.9474	143.4720
A 139 : SER@N	0 : UNN@H8	0 : UNN@O6	4	0.0010	3.3172	132.8935

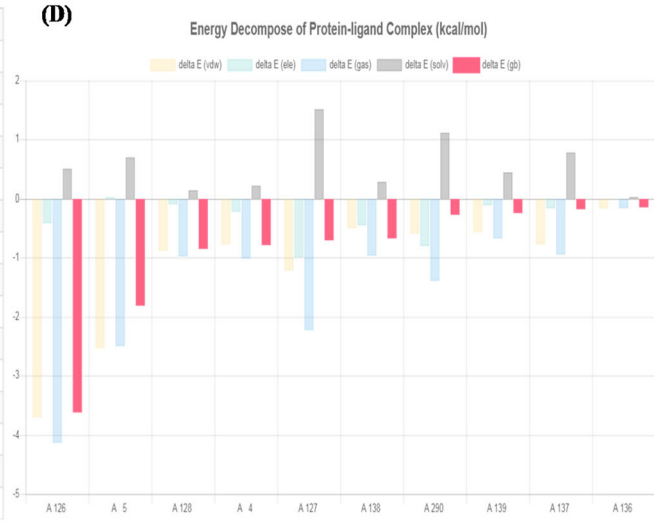

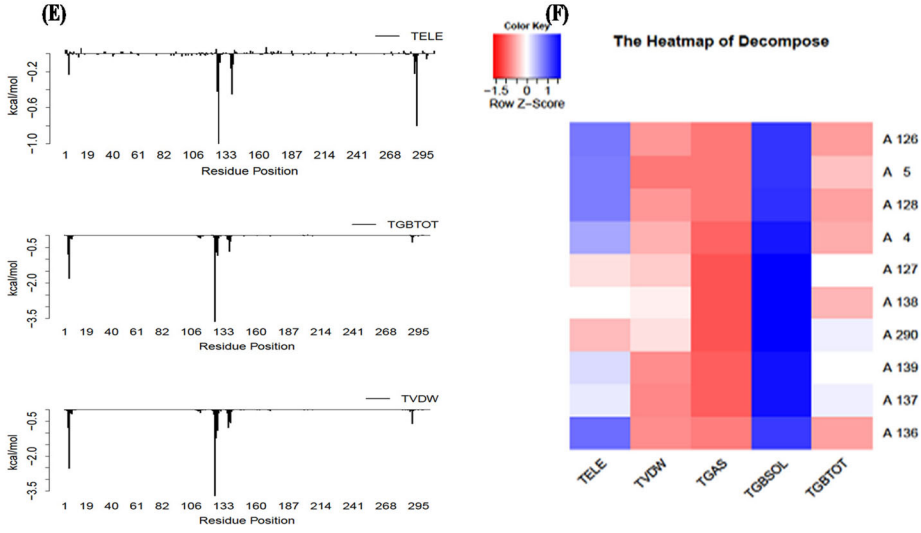

Figure 9. Energy, hydrogen bond analysis and decomposition analysis of SARS-CoV-2 3CLpro (PDB ID: 6Y84) complexed with morin (A) MM/PB(GB)SA result consists of electrostatic energy (ELE), van der Waals contribution (vDW), total gas phase energy (GAS), non-polar and polar contributions to solvation (PBSOL/GBSOL) (B,C) Statistics of hydrogen bonds (D) Energy decompose of protein-ligand complex (kcal/mol) (E) Graphical representation of decompose result (F) Heatmap of decompose.

are known to have a nuclear role in promoting transcription of cytokine genes (Astuti, 2020; Yoshimoto, 2020; https://zhanglab.ccmb.med.umich.edu/COVID-19). Taken together, these reports suggest that morin may act in a similar manner to ivermectin and inhibit nuclear transport. This might prove to be an effective treatment therapy against SARS-CoV-2 (Caly et al., 2012).

To prove an effective drug, a drug-like molecule must reach its target in the body in sufficient concentration and stay there in a bioactive form long enough for the expected biologic events to occur (Daina et al., 2017). In medicinal chemistry, drug development requires evaluation of ADME properties of a drug candidate at an initial phase. The pharmacokinetic properties of morin *versus* reference drugs have been summarized in Table 6. The potential of a drug candidate to cross the BBB is an essential parameter to consider. Skin permeability (Kp) is related to the molecular size and lipophilicity of drug like compounds and negative values of Kp (cm/s) correspond to decreased skin permeability of these compounds (Potts & Guy, 1992). Permeability glycoprotein (P-gp) is an ATP-dependent bioavailability protein pump that removes foreign substances like drugs from biological systems (Montanari & Ecker, 2015). The normal excretion of xenobiotics back into the gut lumen by P-gp pharmacokinetically reduces the efficacy of

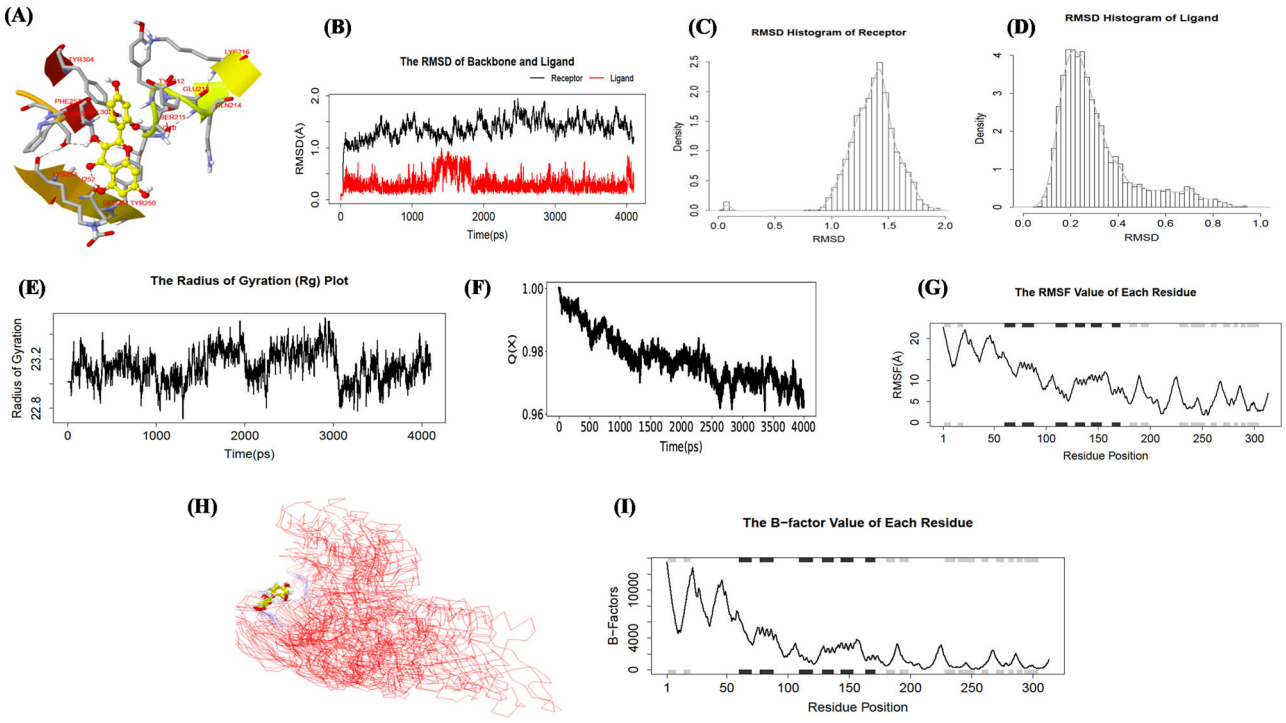

Figure 10. MD Simulation of morin complexed with SARS-CoV-2 papain-like protease PLpro (PDB ID: 6W9C) (A) Ligand-protein conformation (B) RMSD of receptor and ligand (C) RMSD histogram of receptor (D) RMSD histogram of ligand (E) Radius of gyration, Rg value (F) Fraction of native contacts analysis of SARS-CoV-2 PLpro with morin, over a time frame of 4000ps (4 ns) (G) RMSF value of each residue (H) B-factor value (changing from blue to red with increase in value) and (I) B-factor analysis of defined complex.

some pharmaceutical drugs (which are said to be P-gp substrates). Interestingly, some cancer cells have been found to express large amounts of P-gp, further amplifying that effect and rendering these cancers multidrug resistant. Many drugs have been found to inhibit P-gp, typically incidentally rather than as their main mechanism of action; some foods do as well. Such agents act as P-gp inhibitors. In the present study, though baricitinib and morin displayed a more or less similar spectrum of activity against viral and human protein targets and were at par on their druglikeness index, yet baricitinib was found to act as a P-gp substrate (Table 6) that greatly tends to reduce its pharmacodynamics and hence, its efficacy because of elimination by P-gp.

Cytochromes P450 (CYPs) are a superfamily of major metabolic enzymes involved in the biotransformation of xenobiotics (Testa & Kraemer, 2007). The reactions catalyzed by cytochromes P450 are not limited to one type of reaction or one substrate. Instead, each cytochrome P450 enzyme has numerous substrates and catalyzes chemically diverse reactions. Drugs and other xenobiotics can act as both substrates and inhibitors of cytochromes P450. They are involved in the metabolism of most medications and are the mechanism by which most pharmacokinetic drug interactions occur. Important CYP450 enzymes include CYP3A4, CYP1A2, CYP2C9, CYP2C19 and CYP2D6. CYP1A2 is a member of the cytochrome P450 superfamily of enzymes and is a mixed-function oxidase catalyzing many reactions involved in drug metabolism, thus rendering the drug either more or less active. The importance of CYP1A2 for drug interactions has been increasing over the past decade due to the growing number of drugs metabolized by this enzyme (Aniyery et al., 2015). Drugs metabolized by CYP1A2 are called CYP1A2 substrates. Drugs that inhibit CYP1A2 will predictably increase the plasma concentrations of the medications, thus contributing to their bioavailability (Faber et al., 2005).

Cytochrome P450 3A4 (abbreviated CYP3A4) is another important enzyme in the body, found in the liver and in the intestine. It oxidizes xenobiotics such as toxins or drugs, so that they can be removed from the body. While many drugs are deactivated by CYP3A4, there are also some drugs which are activated by the enzyme. CYP2D6, a member of the cytochrome P450 mixed-function oxidase system, is one of the most important enzymes involved in the metabolism of xenobiotics in the body. In particular, CYP2D6 is responsible for the metabolism and elimination of approximately 25% of clinically used drugs *via* the addition or removal of certain functional groups specifically hydroxylation, demethylation, and dealkylation (Wang et al., 2009). Interestingly, both morin and HCQ were found to behave as CYP1A2 and CYP2D6 inhibitors while morin was also found to act as a CYP3A4 inhibitor, which points towards the decreased elimination and metabolism of these compounds by these enzymes and hence increased plasma concentrations as opposed to baricitinib, remdesivir and azithromycin. CYP2C9 is an important cytochrome P450 enzyme with a major role in the oxidation of both xenobiotic and endogenous compounds. CYP2C9 makes up about 18% of the cytochrome P450 protein in liver microsomes. Some 100 therapeutic drugs are metabolized by CYP2C9, including drugs with a narrow therapeutic index.

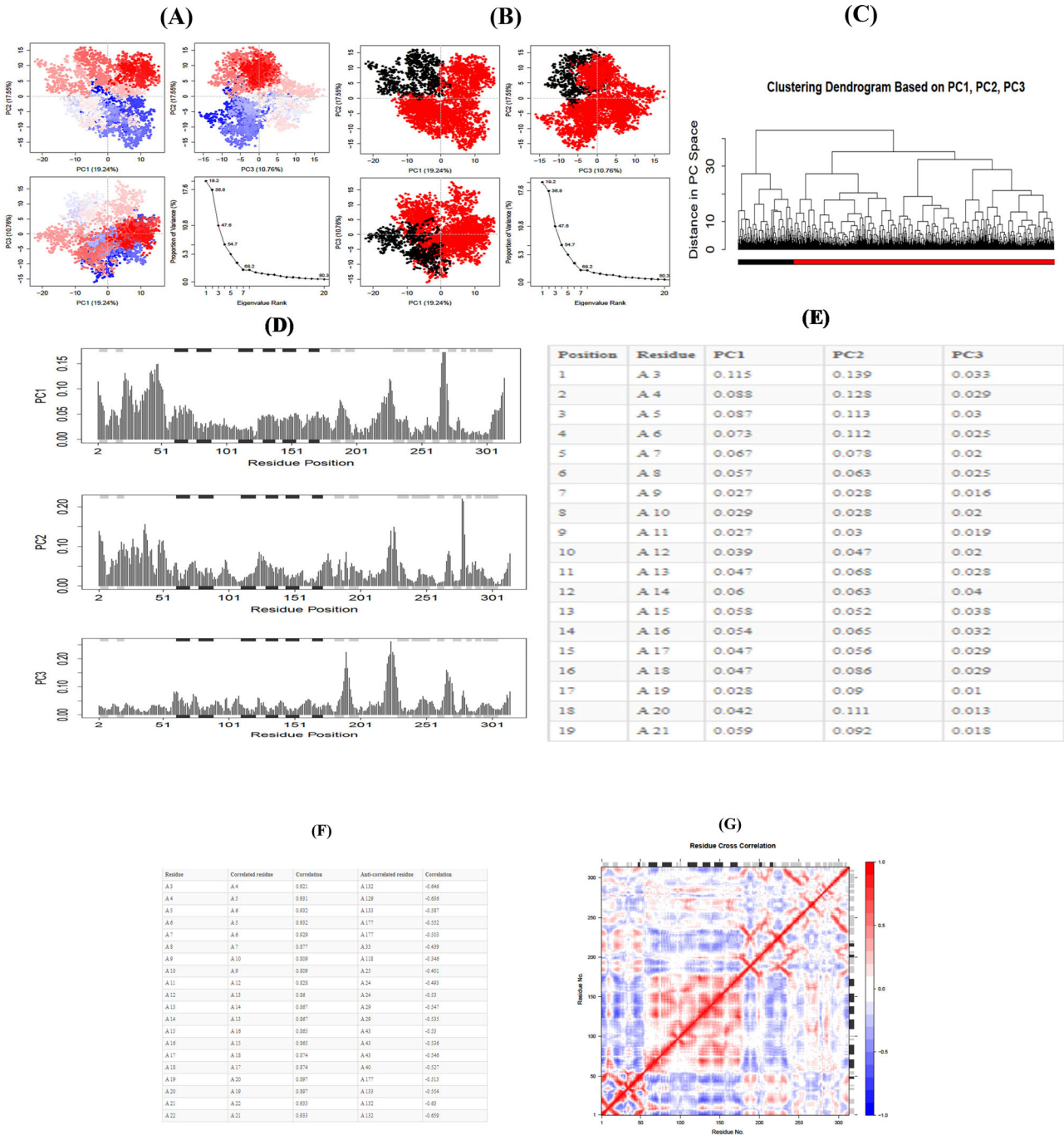

Position	Residue	PC1	PC2	PC3
1	A 3	0.115	0.139	0.033
2	A 4	0.088	0.128	0.029
3	A 5	0.087	0.113	0.03
4	A 6	0.073	0.112	0.025
5	A 7	0.067	0.078	0.02
6	A 8	0.057	0.063	0.025
7	A 9	0.027	0.028	0.016
8	A 10	0.029	0.028	0.02
9	A 11	0.027	0.03	0.019
10	A 12	0.039	0.047	0.02
11	A 13	0.047	0.068	0.028
12	A 14	0.06	0.063	0.04
13	A 15	0.058	0.052	0.038
14	A 16	0.054	0.065	0.032
15	A 17	0.047	0.056	0.029
16	A 18	0.047	0.086	0.029
17	A 19	0.028	0.09	0.01
18	A 20	0.042	0.111	0.013
19	A 21	0.059	0.092	0.018

Residue	Correlated residue	Correlation	Anti-correlated residue	Correlation
A 3	A 4	0.921	A 132	-0.646
A 4	A 5	0.931	A 129	-0.636
A 5	A 6	0.932	A 133	-0.587
A 6	A 5	0.932	A 177	-0.552
A 7	A 6	0.929	A 177	-0.503
A 8	A 7	0.877	A 33	-0.439
A 9	A 10	0.909	A 118	-0.346
A 10	A 9	0.909	A 25	-0.401
A 11	A 12	0.928	A 24	-0.493
A 12	A 13	0.86	A 24	-0.53
A 13	A 14	0.867	A 29	-0.547
A 14	A 13	0.867	A 29	-0.535
A 15	A 16	0.865	A 43	-0.53
A 16	A 15	0.865	A 43	-0.536
A 17	A 18	0.874	A 43	-0.546
A 18	A 17	0.874	A 40	-0.527
A 19	A 20	0.897	A 177	-0.513
A 20	A 19	0.897	A 133	-0.554
A 21	A 22	0.933	A 132	-0.63
A 22	A 21	0.933	A 132	-0.659

Figure 11. PCA of SARS-CoV-2 PLpro (PDB ID: 6W9C) complexed with morin (A) PCA results for Trajectory (B) Simple clustering in PC subspace (C) Clustering dendogram based on PC1, PC2 and PC3 (D) Residue-wise loadings for PC1, PC2 and PC3 (E) Table data showing residue-wise loadings for PC1, PC2 and PC3 and residue number at each position (F) Table showing pair-wise cross-correlation coefficients; higher correlated coefficient value is >0.8 and higher anti-correlated coefficient value is < −0.4 (G) Dynamical Residue Cross-correlation Map; the correlated residues are in blue, anti-correlated residues are in red; the pairwise residues with higher correlated coefficient (>0.8) and with higher anti-correlated coefficient (< −0.4) are linked with light pink and light blue (Int_mod).

Similarly, CYP2C19 catalyzes the metabolism of several drugs, including proton pump inhibitors (PPIs) (e.g., omeprazole, lansoprazole, pantoprazole), antidepressants (e.g., citalopram and amitriptyline), antiplatelet drugs (e.g., clopidogrel), antifungals (e.g., voriconazole) and anticancer compounds (e.g., cyclophosphamide) (https://www.pharmacytimes.com/publications/issue/2007/2007-11/2007-11-8279). In the present study, morin and none of the reference drugs were predicted to behave as CYP2C9 and CYP2C19 inhibitors (Table 6).

5. Concluding remarks

The premise of the present study was to evaluate the flavonol morin for its antiviral efficacy against COVID-19, SARS and MERS, to elucidate its possible modes of action and to evaluate its druglikeness. Morin was found to exhibit good antiviral potential and drug like character without any violations of druglikeness filters. Morin displayed potent binding to a number of viral proteins of SARS-CoV-2, SARS-CoV and

(A)

ELE	VDW	GAS	PBSOL	PBTOT	GBSOL	GBTOT	TS	deltaPB	deltaGB
-4.65	-26.27	-30.92	13.24	-17.68	9.05	-21.87	15.25	-2.43	-6.62

(B)

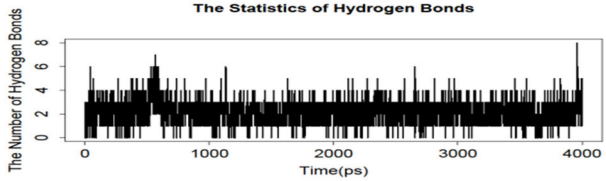

(C)

Acceptor	DonorH	Donor	Frames	Frac	AvgDist	AvgAng
A 214 : GLU@N	0 : UNN@H6	0 : UNN@O4	1	0.0002	3.4915	142.0595
A 212 : SER@OG	0 : UNN@H9	0 : UNN@O7	1	0.0002	3.4276	151.6588
A 217 : LYS@NZ	0 : UNN@H9	0 : UNN@O7	1	0.0002	3.1801	131.3409
A 257 : THR@OG1	0 : UNN@H6	0 : UNN@O4	1	0.0002	3.1001	137.8172
A 214 : GLU@OE2	0 : UNN@H9	0 : UNN@O7	2	0.0005	3.1917	128.6923
A 251 : TYR@OH	0 : UNN@H5	0 : UNN@O3	3	0.0007	3.3957	125.6824
A 251 : TYR@OH	0 : UNN@H8	0 : UNN@O6	3	0.0007	3.3077	135.7736
A 305 : TYR@OH	0 : UNN@H5	0 : UNN@O3	3	0.0007	3.2597	122.5991
A 214 : GLU@N	0 : UNN@H9	0 : UNN@O7	6	0.0015	3.2591	122.2791
A 213 : TYR@N	0 : UNN@H9	0 : UNN@O7	10	0.0024	3.3771	125.5076
A 252 : GLU@O	0 : UNN@H5	0 : UNN@O3	10	0.0024	3.3095	139.8706
A 254 : LYS@NZ	0 : UNN@H7	0 : UNN@O5	13	0.0032	3.3306	129.0826
A 252 : GLU@OE1	0 : UNN@H7	0 : UNN@O5	13	0.0032	3.0722	131.1191
A 252 : GLU@OE2	0 : UNN@H7	0 : UNN@O5	16	0.0039	3.1464	130.0704
A 295 : GLU@OE2	0 : UNN@H7	0 : UNN@O5	30	0.0073	3.2584	127.1768
A 295 : GLU@OE1	0 : UNN@H7	0 : UNN@O5	35	0.0085	3.1897	130.1889
A 212 : SER@OG	0 : UNN@H6	0 : UNN@O4	40	0.0098	3.2098	129.9633

(D)

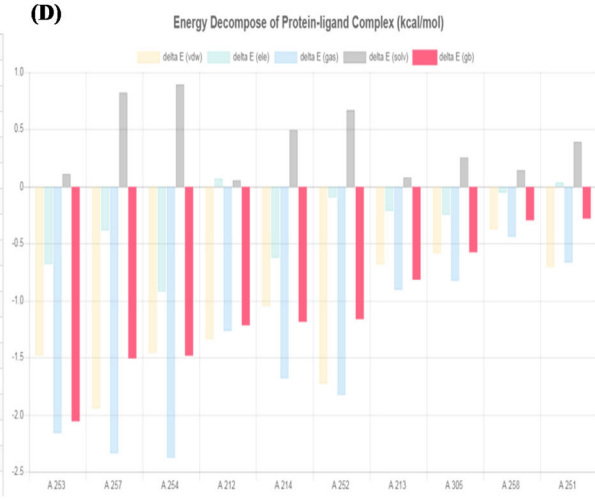

E

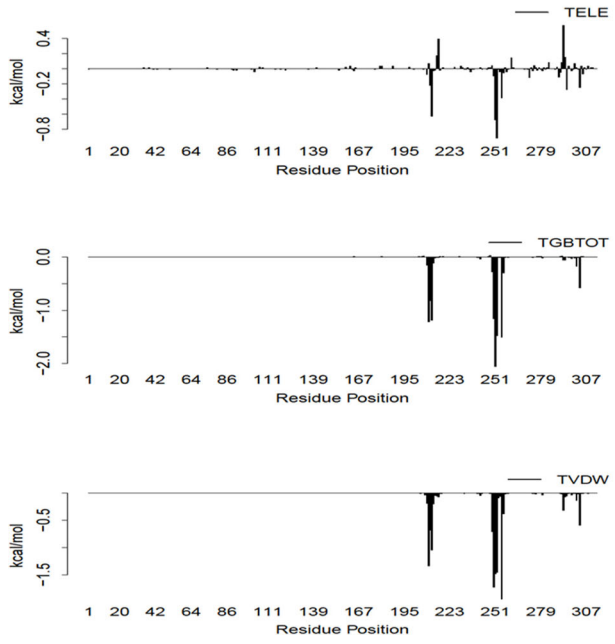

F

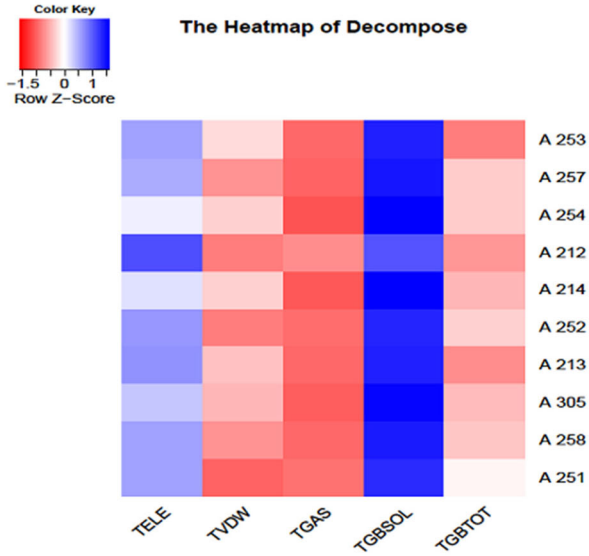

Figure 12. Energy, hydrogen bond analysis and decomposition analysis of SARS-CoV-2 PLpro (PDB ID: 6W9C) complexed with morin (A) MM/PB(GB)SA result consists of electrostatic energy (ELE), van der Waals contribution (vDW), total gas phase energy (GAS), non-polar and polar contributions to solvation (PBSOL/GBSOL) (B,C) Statistics of hydrogen bonds (D) Energy decompose of protein-ligand complex (kcal/mol) (E) Graphical representation of decompose result (F) Heatmap of decompose.

MERS-CoV as well as critical human proteins that are subverted by coronaviruses to either gain entry or perpetuate their life cycle. MD simulation of morin with SARS-CoV-2 3CLPro and PLPro also displayed strong stability at 300 K. Morin also displayed potent anti-inflammatory activity against cytokines IL-6, 8 and 10. Since ARDS is a serious complication in COVID-19, SARS, asthma, COPD and lung emphysema, there is a need to evaluate the efficacy of morin in the control of lung inflammation in these disorders as well as its possible mechanisms of action.

Acknowledgements

The authors gratefully acknowledge Dr. Meraj Ahmad, Professor, Dept. of Sociology, University of Lucknow, Lucknow, India, for being the inspiration and motivation behind the present work in view of his exceptional work and contribution in the area of social sciences, social work, humanities and public health.

Author contributions

Author contributions RA planned, conceptualized and supervised the study whereas AG, RA, SS, AS and AT carried out the computational analyses viz. molecular docking, molecular chemoinformatics and molecular dynamics simulations. RA performed calculations, data analysis and interpretation as well as drafted, edited and revised the manuscript. SS, KY, MAK, AKS and GKS edited, revised and critically reviewed the manuscript whereas BA co-ordinated the overall study design. All authors read and approved the final manuscript.

Disclosure statement

No potential conflict of interest was reported by the authors.

References

Abd El-Aziz, T. M., & Stockand, J. D. (2020). Recent progress and challenges in drug development against COVID-19 coronavirus (SARS-CoV-2)-an update on the status. *Infection, Genetics and Evolution*, *83*, 104327. https://doi.org/10.1016/j.meegid.2020.104327

Ahmad, R. (2019). Steroidal glycoalkaloids from *Solanum nigrum* target cytoskeletal proteins: An *in silico* analysis. *PeerJ*, *7*, e6012. https://doi.org/10.7717/peerj.6012

Andersen, K. G., Rambaut, A., Lipkin, W. I., Holmes, E. C., & Garry, R. F. (2020). The proximal origin of SARS-CoV-2. *Nature Medicine*, *26*, 450–452.

Aniyery, R. B., Sharma, A., & Gupta, A. (2015). Molecular docking studies and *in silico* pharmacokinetic property study of synthesized organotin complex of (1r, 2s, 5r)-2-isopropyl-5-methylcyclohexanol. *Journal of Chemical and Pharmaceutical Sciences*, *9*(4), 2656–2663.

Astuti, I. (2020). Severe acute respiratory syndrome coronavirus 2 (SARS-CoV-2): An overview of viral structure and host response. *Diabetes & Metabolic Syndrome: Clinical Research & Reviews*, *14*(4), 407–412. https://doi.org/10.1016/j.dsx.2020.04.020

Auf'mkolk, M., Koehrle, J., Hesch, R. D., & Cody, V. (1986). Inhibition of rat liver iodothyronine deiodinase. Interaction of aurones with the iodothyronine ligand-binding site. *Journal of Biological Chemistry*, *261*(25), 11623–11628. https://doi.org/10.1016/S0021-9258(18)67288-6

Baell, J. B., & Holloway, G. A. (2010). New substructure filters for removal of pan assay interference compounds (PAINS) from screening libraries and for their exclusion in bioassays. *Journal of Medicinal Chemistry*, *53*(7), 2719–2740. https://doi.org/10.1021/jm901137j

Báez-Santos, Y. M., John, S. E., & Mesecar, A. D. (2015). The SARS-coronavirus papain-like protease: Structure, function and inhibition by designed antiviral compounds. *Antiviral Research*, *115*, 21–38. https://doi.org/10.1016/j.antiviral.2014.12.015

Baricitinib in symptomatic patients infected by COVID-19: An open-label, pilot study (BARI-COVID). ClinicalTrials.gov Identifier: NCT04320277.

Behera, S. M., Mohanta, R. K., Mishra, S. K., Sahu, S. K., Mohanta, L., & Banerjee, M. (2014). *In silico* designing of pyrazol-1-Yl azetidin-2-one derivatives as drug like molecules for possible inhibition of anti microbial 3GI9, 4AE5, 3FHU and 5COX target proteins. *International Journal of Drug Development and Research*, *6*, 78–91.

Benvenuto, D., Giovanetti, M., Ciccozzi, A., Spoto, S., Angeletti, S., & Ciccozzi, M. (2020). The 2019-new coronavirus epidemic: Evidence for virus evolution. *Journal of Medical Virology*, *92*(4), 455–459. https://doi.org/10.1002/jmv.25688

Boseley, S. (2020, April 23). First trial for potential Covid-19 drug shows it has no effect. https://www.theguardian.com/world/2020/apr/23/high-hopes-drug-for-covid-19-treatment-failed-in-full-trial

Bravo, L. (1998). Polyphenols: Chemistry, dietary sources, metabolism, and nutritional significance. *Nutrition Reviews*, *56*(11), 317–333. https://doi.org/10.1111/j.1753-4887.1998.tb01670.x

Brenk, R., Schipani, A., James, D., Krasowski, A., Gilbert, I. H., Frearson, J., & Wyatt, P. G. (2008). Lessons learnt from assembling screening libraries for drug discovery for neglected diseases. *ChemMedChem*, *3*(3), 435–444. https://doi.org/10.1002/cmdc.200700139

Brinkworth, R. I., Stoermer, M. J., & Fairlie, D. P. (1992). Flavones are inhibitors of HIV-1 proteinase. *Biochemical and Biophysical Research Communications*, *188*(2), 631–637. https://doi.org/10.1016/0006-291X(92)91103-W

Caltagirone, S., Ranelletti, F. O., Rinelli, A., Maggiano, N., Colasante, A., Musiani, P., Aiello, F. B., & Piantelli, M. (1997). Interaction with type II estrogen binding sites and antiproliferative activity of tamoxifen and quercetin in human non-small-cell lung cancer. *American Journal of Respiratory Cell and Molecular Biology*, *17*(1), 51–59. https://doi.org/10.1165/ajrcmb.17.1.2728

Caly, L., Druce, J. D., Catton, M. G., Jans, D. A., & Wagstaff, K. M. (2020). The FDA-approved drug ivermectin inhibits the replication of SARS-CoV-2 *in vitro*. *Antiviral Research*, *178*, 104787. https://doi.org/10.1016/j.antiviral.2020.104787

Caly, L., Wagstaff, K. M., & Jans, D. A. (2012). Nuclear trafficking of proteins from RNA viruses: Potential target for antivirals? *Antiviral Research*, *95*(3), 202–206. https://doi.org/10.1016/j.antiviral.2012.06.008

Cao, G., Sofic, E., & Prior, R. L. (1997). Antioxidant and prooxidant behavior of flavonoids: Structure-activity relationships. *Free Radical Biology & Medicine*, *22*(5), 749–760. https://doi.org/10.1016/S0891-5849(96)00351-6

Cazarolli, L. H., Zanatta, L., Alberton, E. H., Figueiredo, M. S. R. B., Folador, P., Damazio, R. G., Pizzolatti, M. G., & Silva, F. R. M. B. (2008). Flavonoids: Prospective drug candidates. *Mini Reviews in Medicinal Chemistry*, *8*(13), 1429–1440. https://doi.org/10.2174/138955708786369564

Chan, J. F., Kok, K. H., Zhu, Z., Chu, H., To, K. K., Yuan, S., & Yuen, K. Y. (2020). Genomic characterization of the 2019 novel human-pathogenic coronavirus isolated from a patient with atypical pneumonia after visiting Wuhan. *Emerging Microbes & Infections*, *9*(1), 221–236. https://doi.org/10.1080/22221751.2020.1719902

Chen, J., Wang, J. B., Yu, C. H., Chen, L. Q., Xu, P., & Yu, W. Y. (2013). Total flavonoids of *Mosla scabra* leaves attenuates lipopolysaccharide-induced acute lung injury via down-regulation of inflammatory signaling in mice . *Journal of Ethnopharmacology*, *148*(3), 835–841. https://doi.org/10.1016/j.jep.2013.05.020

Chen, R., & Zhang, L. (2019). Morin inhibits colorectal tumor growth through inhibition of NF-κB signaling pathway. *Immunopharmacology and Immunotoxicology*, *41*(6), 622–629. https://doi.org/10.1080/08923973.2019.1688344

Ciurli, S., Benini, S., Rypniewski, W. R., Wilson, K. S., Miletti, S., & Mangani, S. (1999). Structural properties of the nickel ions in urease: Novel insights into the catalytic and inhibition mechanisms. *Coordination Chemistry Reviews*, *190–192*, 331–355. https://doi.org/10.1016/S0010-8545(99)00093-4

Cody, V., Middleton, E., & Harborne, J. B. (1986). *Plant flavonoids in biology and medicine: biochemical, pharmacological, and structure-activity relationships*. Proceedings of a symposium held in Buffalo, New York, July 22–26, 1985.

Coombs, K. E., Mann, E. R., Edwards, J. U., & Brown, D. T. (1981). Effects of chloroquine and cytochalasin B on the infection of cells by Sindbis virus and vesicular stomatitis virus. *Journal of Virology*, *37*(3), 1060–1065. https://doi.org/10.1128/JVI.37.3.1060-1065.1981

Costedoat-Chalumeau, N., Dunogué, B., Leroux, G., Morel, N., Jallouli, M., Le Guern, V., Piette, J. C., Brézin, A. P., Melles, R. B., & Marmor, M. F. (2015). A critical review of the effects of hydroxychloroquine and chloroquine on the eye. *Clinical Reviews in Allergy & Immunology*, *49*(3), 317–326. https://doi.org/10.1007/s12016-015-8469-8

Daina, A., Michielin, O., & Zoete, V. (2017). SwissADME: A free web tool to evaluate pharmacokinetics, drug-likeness and medicinal chemistry

friendliness of small molecules. *Scientific Reports*, *7*, 42717. https://doi.org/10.1038/srep42717

Daina, A., & Zoete, V. (2016). A BOILED-egg to predict gastrointestinal absorption and brain penetration of small molecules. *ChemMedChem*, *11*(11), 1117–1121. https://doi.org/10.1002/cmdc.201600182

Delogu, I., & de Lamballerie, X. (2011). Chikungunya disease and chloroquine treatment. *Journal of Medical Virology*, *83*(6), 1058–1059. https://doi.org/10.1002/jmv.22019

Dilshara, M. G., Jayasooriya, R. G., Lee, S., Choi, Y. H., & Kim, G. Y. (2016). Morin downregulates nitric oxide and prostaglandin E2 production in LPS-stimulated BV2 microglial cells by suppressing NF-κB activity and activating HO-1 induction. *Environmental Toxicology and Pharmacology*, *44*, 62–68. https://doi.org/10.1016/j.etap.2016.04.010

Dolinsky, T. J., Czodrowski, P., Li, H., Nielsen, J. E., Jensen, J. H., Klebe, G., & Baker, N. A. (2007). PDB2PQR: Expanding and upgrading automated preparation of biomolecular structures for molecular simulations. *Nucleic Acids Research*, *35*(Web Server issue), W522–W525. https://doi.org/10.1093/nar/gkm276

Dong, N., Yang, X., Ye, L., Chen, K., Chan, E. W., Yang, M., & Chen, S. (2020). Genomic and protein structure modelling analysis depicts the origin and infectivity of 2019-nCoV, a new coronavirus which caused a pneumonia outbreak in Wuhan, China. *BioRxiv*.

Dowall, S. D., Bosworth, A., Watson, R., Bewley, K., Taylor, I., Rayner, E., Hunter, L., Pearson, G., Easterbrook, L., Pitman, J., Hewson, R., & Carroll, M. W. (2015). Chloroquine inhibited Ebola virus replication *in vitro* but failed to protect against infection and disease in the *in vivo* guinea pig g model. *The Journal of General Virology*, *96*(12), 3484–3492. https://doi.org/10.1099/jgv.0.000309

Egan, W. J., Merz, K. M., & Baldwin, J. J. (2000). Prediction of drug absorption using multivariate statistics. *Journal of Medicinal Chemistry*, *43*(21), 3867–3877. https://doi.org/10.1021/jm000292e

Elliott, A. J., Scheiber, S. A., Thomas, C., & Pardini, R. S. (1992). Inhibition of glutathione reductase by flavonoids: A structure-activity study. *Biochemical Pharmacology*, *44*(8), 1603–1608. https://doi.org/10.1016/0006-2952(92)90478-2

Ertl, P., Roggo, S., & Schuffenhauer, A. (2008). Natural product-likeness score and its application for prioritization of compound libraries. *Journal of Chemical Information and Modeling*, *48*(1), 68–74. https://doi.org/10.1021/ci700286x

Ertl, P., & Schuffenhauer, A. (2009). Estimation of synthetic accessibility score of drug-like molecules based on molecular complexity and fragment contributions. *Journal of Cheminformatics*, *1*(1), 8. https://doi.org/10.1186/1758-2946-1-8

Faber, M. S., Jetter, A., & Fuhr, U. (2005). Assessment of CYP1A2 activity in clinical practice: Why, how, and when? *Basic & Clinical Pharmacology & Toxicology*, *97*(3), 125–134. https://doi.org/10.1111/j.1742-7843.2005.pto_973160.x

Falzarano, D., Safronetz, D., Prescott, J., Marzi, A., Feldmann, F., & Feldmann, H. (2015). Lack of protection against ebola virus from chloroquine in mice and hamsters. *Emerging Infectious Diseases*, *21*(6), 1065–1067. https://doi.org/10.3201/eid2106.150176

Fang, S. H., Hou, Y. C., Chang, W. C., Hsiu, S. L., Chao, P. D., & Chiang, B. L. (2003). Morin sulfates/glucuronides exert anti-inflammatory activity on activated macrophages and decreased the incidence of septic shock. *Life Sciences*, *74*(6), 743–756. https://doi.org/10.1016/j.lfs.2003.07.017

Ferner, R. E., & Aronson, J. K. (2020). Chloroquine and hydroxychloroquine in covid-19. *BMJ*, 2020, 369.

Ferriola, P. C., Cody, V., & Middleton, E., Jr. (1989). Protein kinase C inhibition by plant flavonoids: Kinetic mechanisms and structure-activity relationships. *Biochemical Pharmacology*, *38*(10), 1617–1624. https://doi.org/10.1016/0006-2952(89)90309-2

Franova, S., Kazimierova, I., Pappova, L., Joskova, M., Plank, L., & Sutovska, M. (2016). Bronchodilatory, antitussive and anti-inflammatory effect of morin in the setting of experimentally induced allergic asthma. *The Journal of Pharmacy and Pharmacology*, *68*(8), 1064–1072. https://doi.org/10.1111/jphp.12576

Frisk-Holmberg, M., Bergqvist, Y., & Englund, U. (1983). Chloroquine intoxication. *British Journal of Clinical Pharmacology*, *15*(4), 502–503. https://doi.org/10.1111/j.1365-2125.1983.tb01540.x

Galvez, J., Coelho, G., Crespo, M. E., Cruz, T., Rodríguez-Cabezas, M. E., Concha, A., Gonzalez, M., & Zarzuelo, A. (2001). Intestinal anti-inflammatory activity of morin on chronic experimental colitis in the rat. *Alimentary Pharmacology & Therapeutics*, *15*(12), 2027–2039. https://doi.org/10.1046/j.1365-2036.2001.01133.x

Ghose, A. K., Viswanadhan, V. N., & Wendoloski, J. J. (1999). A knowledge-based approach in designing combinatorial or medicinal chemistry libraries for drug discovery. 1. A qualitative and quantitative characterization of known drug databases. *Journal of Combinatorial Chemistry*, *1*(1), 55–68. Jan 12 https://doi.org/10.1021/cc9800071

Gong, J., Dong, H., Xia, S. Q., Huang, Y. Z., Wang, D., Zhao, Y., Liu, W., Tu, S., Zhang, M., Wang, Q., & Lu, F. (2020). Correlation analysis between disease severity and inflammation-related parameters in patients with COVID-19 pneumonia. *MedRxiv*.

Gorbalenya, A. E., Baker, S. C., Baric, R. S., de Groot, R. J., Drosten, C., Gulyaeva, A. A., Haagmans, B. L., Lauber, C., Leontovich, A. M., Neuman, B. W., & Penzar, D. (2020). The species severe acute respiratory syndrome related coronavirus: Classifying 2019-nCoV and naming it SARS-CoV-2. *Nature Microbiology*, *5*, 536–544.

Götz, V., Magar, L., Dornfeld, D., Giese, S., Pohlmann, A., Höper, D., Kong, B. W., Jans, D. A., Beer, M., Haller, O., & Schwemmle, M. (2016). Influenza A viruses escape from MxA restriction at the expense of efficient nuclear vRNP import. *Scientific Reports*, *6*(1), 25428–25425. https://doi.org/10.1038/srep25428

Hann, M. M., & Keserü, G. M. (2012). Finding the sweet spot: The role of nature and nurture in medicinal chemistry. *Nature Reviews. Drug Discovery*, *11*(5), 355–365. https://doi.org/10.1038/nrd3701

Huang, C., Wang, Y., Li, X., Ren, L., Zhao, J., Hu, Y., Zhang, L., Fan, G., Xu, J., Gu, X., Cheng, Z., Yu, T., Xia, J., Wei, Y., Wu, W., Xie, X., Yin, W., Li, H., Liu, M., … Cao, B. (2020). Clinical features of patients infected with 2019 novel coronavirus in Wuhan, China. *The Lancet*, *395*(10223), 497–506. https://doi.org/10.1016/S0140-6736(20)30183-5

Jans, D. A., Martin, A. J., & Wagstaff, K. M. (2019). Inhibitors of nuclear transport. *Current Opinion in Cell Biology*, *58*, 50–60. https://doi.org/10.1016/j.ceb.2019.01.001

Jayaseelan, K. V., Moreno, P., Truszkowski, A., Ertl, P., & Steinbeck, C. (2012). Natural product-likeness score revisited: An open-source, open-data implementation. *BMC Bioinformatics*, *13*(1), 106. https://doi.org/10.1186/1471-2105-13-106

Jih, T. K. (2005). Acute respiratory distress syndrome (ARDS) and severe acute respiratory syndrome (SARS): Are we speaking different languages? *Journal of the Chinese Medical Association*, *68*(1), 1–3. https://doi.org/10.1016/S1726-4901(09)70123-6

Kaiser, K. L., & Valdmanis, I. (1982). Apparent octanol/water partition coefficients of pentachlorophenol as a function of pH. *Canadian Journal of Chemistry*, *60*(16), 2104–2106. https://doi.org/10.1139/v82-300

Kamitani, W., Narayanan, K., Huang, C., Lokugamage, K., Ikegami, T., Ito, N., Kubo, H., & Makino, S. (2006). Severe acute respiratory syndrome coronavirus nsp1 protein suppresses host gene expression by promoting host mRNA degradation. *Proceedings of the National Academy of Sciences of the United States of America*, *103*(34), 12885–12890. https://doi.org/10.1073/pnas.0603144103

Kannan, S., Ali, P. S., Sheeza, A., & Hemalatha, K. (2020). COVID-19 (Novel Coronavirus 2019) - Recent trends. *European Review for Medical and Pharmacological Sciences*, *24*(4), 2006–2011. https://doi.org/10.26355/eurrev_202002_20378

Kataria, R., & Khatkar, A. (2019). Molecular docking, synthesis, kinetics study, structure-activity relationship and ADMET analysis of morin analogous as *Helicobacter pylori* urease inhibitors. *BMC Chemistry*, *13*(1), 45. https://doi.org/10.1186/s13065-019-0562-2

Keyaerts, E., Li, S., Vijgen, L., Rysman, E., Verbeeck, J., Van Ranst, M., & Maes, P. (2009). Antiviral activity of chloroquine against human coronavirus OC43 infection in newborn mice. *Antimicrobial Agents and Chemotherapy*, *53*(8), 3416–3421. https://doi.org/10.1128/AAC.01509-08

Keyaerts, E., Vijgen, L., Maes, P., Neyts, J., & Van Ranst, M. (2004). *In vitro* inhibition of severe acute respiratory syndrome coronavirus by chloroquine. *Biochemical and Biophysical Research Communications*, *323*(1), 264–268. https://doi.org/10.1016/j.bbrc.2004.08.085

Khaerunnisa, S., Kurniawan, H., Awaluddin, R., Suhartati, S., & Soetjipto, S. (2020). Potential inhibitor of COVID-19 main protease (Mpro) from several medicinal plant compounds by molecular docking study. https://doi.org/10.20944/preprints202003.0226.v1

Khan, T., Azad, I., Ahmad, R., Raza, S., Dixit, S., Joshi, S., & Khan, A. R. (2018). Synthesis, characterization, computational studies and biological activity evaluation of Cu, Fe, Co and Zn complexes with 2-butanone thiosemicarbazone and 1, 10-phenanthroline ligands as anticancer and antibacterial agents. *EXCLI Journal*, *17*, 331.

Khazan, M., & Hdayati, M. (2014). The role of nitric oxide in health and diseases. *Scimetr*, *3*(1), e87393. https://doi.org/10.5812/scimetr.20987

Kim, J. W., Lee, J. H., Hwang, B. Y., Mun, S. H., Ko, N. Y., Kim, D. K., Kim, B., Kim, H. S., Kim, Y. M., & Choi, W. S. (2009). Morin inhibits Fyn kinase in mast cells and IgE-mediated type I hypersensitivity response *in vivo*. *Biochemical Pharmacology*, *77*(9), 1506–1512. https://doi.org/10.1016/j.bcp.2009.01.019

Koehrle, J., Fang, S. L., Yang, Y., Irmscher, K., Hesch, R. D., Pino, S., Alex, S., & Braverman, L. E. (1989). Rapid effects of the flavonoid EMD 21388 on serum thyroid hormone binding and thyrotropin regulation in the rat. *Endocrinology*, *125*(1), 532–537. https://doi.org/10.1210/endo-125-1-532

Lee, H. S., Jung, K. H., Hong, S. W., Park, I. S., Lee, C., Han, H. K., Lee, D. H., & Hong, S. S. (2008). Morin protects acute liver damage by carbon tetrachloride (CCl(4)) in rat. *Archives of Pharmacal Research*, *31*(9), 1160–1165. https://doi.org/10.1007/s12272-001-1283-5

Lee, K. H., & Yoo, C. G. (2013). Simultaneous inactivation of GSK-3β suppresses quercetin-induced apoptosis by inhibiting the JNK pathway. *American Journal of Physiology. Lung Cellular and Molecular Physiology*, *304*(11), L782–9. https://doi.org/10.1152/ajplung.00348.2012

Lee, M. H., Cha, H.-J., Choi, E. O., Han, M. H., Kim, S. O., Kim, G.-Y., Hong, S. H., Park, C., Moon, S.-K., Jeong, S.-J., Jeong, M.-J., Kim, W.-J., & Choi, Y. H. (2017). Antioxidant and cytoprotective effects of morin against hydrogen peroxide-induced oxidative stress are associated with the induction of Nrf-2-mediated HO-1 expression in V79-4 Chinese hamster lung fibroblasts. *International Journal of Molecular Medicine*, *39*(3), 672–680. https://doi.org/10.3892/ijmm.2017.2871

Li, H. W., Zou, T. B., Jia, Q., Xia, E. Q., Cao, W. J., Liu, W., He, T. P., & Wang, Q. (2016). Anticancer effects of morin-7-sulphate sodium, a flavonoid derivative, in mouse melanoma cells. *Biomedicine & Pharmacotherapy = Biomedecine & Pharmacotherapie*, *84*, 909–916. https://doi.org/10.1016/j.biopha.2016.10.001

Lim, H. J., Jin, H. G., Woo, E. R., Lee, S. K., & Kim, H. P. (2013). The root barks of *Morus alba* and the flavonoid constituents inhibit airway inflammation. *Journal of Ethnopharmacology*, *149*(1), 169–175. https://doi.org/10.1016/j.jep.2013.06.017

Lipinski, C. A., Lombardo, F., Dominy, B. W., & Feeney, P. J. (1997). Experimental and computational approaches to estimate solubility and permeability in drug discovery and development settings. *Advanced Drug Delivery Reviews*, *23*(1–3), 3–25. https://doi.org/10.1016/S0169-409X(96)00423-1

Liu, C., Zhou, Q., Li, Y., Garner, L. V., Watkins, S. P., Carter, L. J., Smoot, J., Gregg, A. C., Daniels, A. D., Jervey, S., & Albaiu, D. (2020). Research and development on therapeutic agents and vaccines for COVID-19 and related human coronavirus diseases. *ACS Central Science*, *6*(3), 315–331.

Liu, W., Morse, J. S., Lalonde, T., & Xu, S. (2020). Learning from the past: Possible urgent prevention and treatment options for severe acute respiratory infections caused by 2019-nCoV. *ChemBioChem*.

Lokugamage, K. G., Narayanan, K., Nakagawa, K., Terasaki, K., Ramirez, S. I., Tseng, C. T., & Makino, S. (2015). Middle East respiratory syndrome coronavirus nsp1 inhibits host gene expression by selectively targeting mRNAs transcribed in the nucleus while sparing mRNAs of cytoplasmic origin. *Journal of Virology*, *89*(21), 10970–10981. https://doi.org/10.1128/JVI.01352-15

Lovering, F., Bikker, J., & Humblet, C. (2009). Escape from Flatland: Increasing saturation as an approach to improving clinical success. *Journal of Medicinal Chemistry*, *52*(21), 6752–6756. https://doi.org/10.1021/jm901241e

Lu, R., Zhao, X., Li, J., Niu, P., Yang, B., Wu, H., Wang, W., Song, H., Huang, B., Zhu, N., Bi, Y., Ma, X., Zhan, F., Wang, L., Hu, T., Zhou, H., Hu, Z., Zhou, W., Zhao, L., … Tan, W. (2020). Genomic characterisation and epidemiology of 2019 novel coronavirus: Implications for virus origins and receptor binding. *The Lancet*, *395*(10224), 565–574. https://doi.org/10.1016/S0140-6736(20)30251-8

Lundberg, L., Pinkham, C., Baer, A., Amaya, M., Narayanan, A., Wagstaff, K. M., Jans, D. A., & Kehn-Hall, K. (2013). Nuclear import and export inhibitors alter capsid protein distribution in mammalian cells and reduce Venezuelan Equine Encephalitis Virus replication. *Antiviral Research*, *100*(3), 662–672. https://doi.org/10.1016/j.antiviral.2013.10.004

Martin, Y. C. (2005). A bioavailability score. *Journal of Medicinal Chemistry*, *48*(9), 3164–3170. https://doi.org/10.1021/jm0492002

Meanwell, N. A. (2016). Improving drug design: An update on recent applications of efficiency metrics, strategies for replacing problematic elements, and compounds in nontraditional drug space. *Chemical Research in Toxicology*, *29*(4), 564–616. https://doi.org/10.1021/acs.chemrestox.6b00043

Middleton, E., Jr., & Drzewiecki, G. (1982). Effects of flavonoids and transitional metal cations on antigen-induced histamine release from human basophils. *Biochemical Pharmacology*, *31*(7), 1449–1453. https://doi.org/10.1016/0006-2952(82)90044-2

Mobley, H. L., & Hausinger, R. P. (1989). Microbial ureases: Significance, regulation, and molecular characterization. *Microbiological Reviews*, *53*(1), 85–108. https://doi.org/10.1128/MMBR.53.1.85-108.1989

Montanari, F., & Ecker, G. F. (2015). Prediction of drug-ABC-transporter interaction-Recent advances and future challenges. *Advanced Drug Delivery Reviews*, *86*, 17–26. https://doi.org/10.1016/j.addr.2015.03.001

Muegge, I., Heald, S. L., & Brittelli, D. (2001). Simple selection criteria for drug-like chemical matter. *Journal of Medicinal Chemistry*, *44*(12), 1841–1846. https://doi.org/10.1021/jm015507e

Nakagawa, K., Lokugamage, K. G., & Makino, S. (2016). *Viral and cellular mRNA translation in coronavirus-infected cells. InAdvances in virus research* (Vol. 96, pp. 165–192). Academic Press.

O'Leary, K. A., de Pascual-Teresa, S., de Pascual-Tereasa, S., Needs, P. W., Bao, Y.-P., O'Brien, N. M., & Williamson, G. (2004). Effect of flavonoids and vitamin E on cyclooxygenase-2 (COX-2) transcription. Mutation Research/Fundamental and Molecular Mechanisms of Mutagenesis. *Mutation Research*, *551*(1–2), 245–254. https://doi.org/10.1016/j.mrfmmm.2004.01.015

Pal, R., Chaudhary, M. J., Tiwari, P. C., Babu, S., & Pant, K. K. (2015). Protective role of theophylline and their interaction with nitric oxide (NO) in adjuvant-induced rheumatoid arthritis in rats. *International Immunopharmacology*, *29*(2), 854–862. https://doi.org/10.1016/j.intimp.2015.08.031

Pallister, J., Middleton, D., Crameri, G., Yamada, M., Klein, R., Hancock, T. J., Foord, A., Shiell, B., Michalski, W., Broder, C. C., & Wang, L. F. (2009). Chloroquine administration does not prevent Nipah virus infection and disease in ferrets. *Journal of Virology*, *83*(22), 11979–11982. https://doi.org/10.1128/JVI.01847-09

Paoli, P., Cirri, P., Caselli, A., Ranaldi, F., Bruschi, G., Santi, A., & Camici, G. (2013). The insulin-mimetic effect of Morin: A promising molecule in diabetes treatment. *Biochimica et Biophysica Acta*, *1830*(4), 3102–3111. https://doi.org/10.1016/j.bbagen.2013.01.017

Potts, R. O., & Guy, R. H. (1992). Predicting skin permeability. *Pharmaceutical Research*, *9*(5), 663–669. https://doi.org/10.1023/A:1015810312465

Pryor, M. J., Rawlinson, S. M., Butcher, R. E., Barton, C. L., Waterhouse, T. A., Vasudevan, S. G., Bardin, P. G., Wright, P. J., Jans, D. A., & Davidson, A. D. (2007). Nuclear localization of dengue virus nonstructural protein 5 Through Its Importin alpha/beta-recognized nuclear localization sequences is integral to viral infection. *Traffic (Copenhagen, Denmark)*, *8*(7), 795–807. https://doi.org/10.1111/j.1600-0854.2007.00579.x

Rahmati, M., & Moosavi, M. A. (2020). Cytokine-targeted therapy in severely ill COVID-19 patients: Options and cautions. *EJMO*, *4*(2), 179–181.

Ranelletti, F. O., Ricci, R., Larocca, L. M., Maggiano, N., Capelli, A., Scambia, G., Benedetti-Panici, P., Mancuso, S., Rumi, C., & Piantelli, M. (1992). Growth-inhibitory effect of quercetin and presence of type-II estrogen-binding sites in human colon-cancer cell lines and primary

colorectal tumors. *International Journal of Cancer*, *50*(3), 486–492. https://doi.org/10.1002/ijc.2910500326

Richardson, P., Griffin, I., Tucker, C., Smith, D., Oechsle, O., Phelan, A., Rawling, M., Savory, E., & Stebbing, J. (2020). Baricitinib as potential treatment for 2019-nCoV acute respiratory disease. *Lancet (London, England)*, *395*(10223), e30–e31. https://doi.org/10.1016/S0140-6736(20)30304-4

Ritchie, T. J., Ertl, P., & Lewis, R. (2011). The graphical representation of ADME-related molecule properties for medicinal chemists. *Drug Discovery Today*, *16*(1–2), 65–72. https://doi.org/10.1016/j.drudis.2010.11.002

Rubenfeld, G. D. (2003). Is SARS just ARDS? *JAMA*, *290*(3), 397–399. https://doi.org/10.1001/jama.290.3.397-a

Shereen, M. A., Khan, S., Kazmi, A., Bashir, N., & Siddique, R. (2020). COVID-19 infection: Origin, transmission, and characteristics of human coronaviruses. *Journal of Advanced Research*, *24*, 91–98. https://doi.org/10.1016/j.jare.2020.03.005

Sujoy, B., & Aparna, A. (2013). Potential clinical significance of urease enzyme. *European Scientific Journal*, *9*(21). https://doi.org/10.19044/esj.2013.v9n21p%p

Tan, Y. W., Yam, W. K., Sun, J., & Chu, J. J. (2018). An evaluation of chloroquine as a broad-acting antiviral against hand, foot and mouth disease. *Antiviral Research*, *149*, 143–149. https://doi.org/10.1016/j.antiviral.2017.11.017

Tay, M. Y., Fraser, J. E., Chan, W. K., Moreland, N. J., Rathore, A. P., Wang, C., Vasudevan, S. G., & Jans, D. A. (2013). Nuclear localization of dengue virus (DENV) 1-4 non-structural protein 5; protection against all 4 DENV serotypes by the inhibitor Ivermectin . *Antiviral Research*, *99*(3), 301–306. https://doi.org/10.1016/j.antiviral.2013.06.002

Teague, S. J., Davis, A. M., Leeson, P. D., & Oprea, T. (1999). The design of leadlike combinatorial libraries. *Angewandte Chemie International Edition*, *38*(24), 3743–3748. https://doi.org/10.1002/(SICI)1521-3773(19991216)38:24<3743::AID-ANIE3743>3.0.CO;2-U

Testa, B., & Kraemer, S. D. (2007). The biochemistry of drug metabolism – An introduction-Testa-2007-chemistry & biodiversity-wiley online library. *Chemistry and Biodiversity*, *4*(3), 257–405.

Touret, F., & de Lamballerie, X. (2020). Of chloroquine and COVID-19. *Antiviral Research*, *177*, 104762. https://doi.org/10.1016/j.antiviral.2020.104762

Trott, O., & Olson, A. J. (2010). AutoDock Vina: Improving the speed and accuracy of docking with a new scoring function, efficient optimization, and multithreading. *Journal of Computational Chemistry*, *31*(2), 455–461. https://doi.org/10.1002/jcc.21334

Tseng, T. L., Chen, M. F., Tsai, M. J., Hsu, Y. H., Chen, C. P., & Lee, T. J. (2012). Oroxylin-A rescues LPS-induced acute lung injury via regulation of NF-κB signaling pathway in rodents . *PLoS One*, *7*(10), e47403. https://doi.org/10.1371/journal.pone.0047403

Ursu, O., Rayan, A., Goldblum, A., & Oprea, T. I. (2011). Understanding drug-likeness. *WIREs Computational Molecular Science*, *1*(5), 760–781. https://doi.org/10.1002/wcms.52

Veber, D. F., Johnson, S. R., Cheng, H. Y., Smith, B. R., Ward, K. W., & Kopple, K. D. (2002). Molecular properties that influence the oral bioavailability of drug candidates. *Journal of Medicinal Chemistry*, *45*(12), 2615–2623. https://doi.org/10.1021/jm020017n

Varma, S.D. (1986). Inhibition of aldose reductase by flavonoids: possible attenuation of diabetic complications. *Proceedings of Clinical Biology Research*, *213*, 343.

Verma, A. (2012). Lead finding from *Phyllanthus debelis* with hepatoprotective potentials. *Asian Pacific Journal of Tropical Biomedicine*, *2*(3), S1735–S1737. https://doi.org/10.1016/S2221-1691(12)60486-9

Vigerust, D. J., & McCullers, J. A. (2007). Chloroquine is effective against influenza A virus *in vitro* but not *in vivo*. *Influenza and Other Respiratory Viruses*, *1*(5–6), 189–192. https://doi.org/10.1111/j.1750-2659.2007.00027.x

Wagstaff, K. M., Rawlinson, S. M., Hearps, A. C., & Jans, D. A. (2011). An AlphaScreen®-based assay for high-throughput screening for specific inhibitors of nuclear import. *Journal of Biomolecular Screening*, *16*(2), 192–200. https://doi.org/10.1177/1087057110390360

Wagstaff, K. M., Sivakumaran, H., Heaton, S. M., Harrich, D., & Jans, D. A. (2012). Ivermectin is a specific inhibitor of importin α/β-mediated nuclear import able to inhibit replication of HIV-1 and dengue virus. *The Biochemical Journal*, *443*(3), 851–856. https://doi.org/10.1042/BJ20120150

Wang, B., Yang, L. P., Zhang, X. Z., Huang, S. Q., Bartlam, M., & Zhou, S. F. (2009). New insights into the structural characteristics and functional relevance of the human cytochrome P450 2D6 enzyme. *Drug Metabolism Reviews*, *41*(4), 573–643. https://doi.org/10.1080/03602530903118729

Wang, M., Cao, R., Zhang, L., Yang, X., Liu, J., Xu, M., Shi, Z., Hu, Z., Zhong, W., & Xiao, G. (2020). Remdesivir and chloroquine effectively inhibit the recently emerged novel coronavirus (2019-nCoV) *in vitro*. *Cell Research*, *30*(3), 269–271. https://doi.org/10.1038/s41422-020-0282-0

Warren, T. K., Jordan, R., Lo, M. K., Ray, A. S., Mackman, R. L., Soloveva, V., Siegel, D., Perron, M., Bannister, R., Hui, H. C., Larson, N., Strickley, R., Wells, J., Stuthman, K. S., Van Tongeren, S. A., Garza, N. L., Donnelly, G., Shurtleff, A. C., Retterer, C. J., … Bavari, S. (2016). Therapeutic efficacy of the small molecule GS-5734 against Ebola virus in rhesus monkeys. *Nature*, *531*(7594), 381–385. https://doi.org/10.1038/nature17180

Warren, T., Jordan, R., Lo, M., Soloveva, V., Ray, A., Bannister, R., Mackman, R., Perron, M., Stray, K., Feng, J., Xu, Y., Wells, J., Stuthman, K., Welch, L., Doerffler, E., Zhang, L., Chun, K., Hui, H., Neville, S., … Bavari, S. (2015). Nucleotide prodrug GS-5734 is a broad-spectrum filovirus inhibitor that provides complete therapeutic protection against the development of Ebola virus disease (EVD) in infected non-human primates. *Open Forum Infectious Diseases*, *2*(suppl_1), LB-2. https://doi.org/10.1093/ofid/ofv130.02

Weiss, S. R., & Navas-Martin, S. (2005). Coronavirus pathogenesis and the emerging pathogen severe acute respiratory syndrome coronavirus. *Microbiology and Molecular Biology Reviews: MMBR*, *69*(4), 635–664. https://doi.org/10.1128/MMBR.69.4.635-664.2005

Weseler, A. R., Geraets, L., Moonen, H. J., Manders, R. J., van Loon, L. J., Pennings, H. J., Wouters, E. F., Bast, A., & Hageman, G. J. (2009). Poly (ADP-ribose) polymerase-1–inhibiting flavonoids attenuate cytokine release in blood from male patients with chronic obstructive pulmonary disease or type 2 diabetes. *The Journal of Nutrition*, *139*(5), 952–957. https://doi.org/10.3945/jn.108.102756

Wu, F., Zhao, S., Yu, B., Chen, Y.-M., Wang, W., Song, Z.-G., Hu, Y., Tao, Z.-W., Tian, J.-H., Pei, Y.-Y., Yuan, M.-L., Zhang, Y.-L., Dai, F.-H., Liu, Y., Wang, Q.-M., Zheng, J.-J., Xu, L., Holmes, E. C., & Zhang, Y.-Z. (2020). A new coronavirus associated with human respiratory disease in China. *Nature*, *579*(7798), 265–269. https://doi.org/10.1038/s41586-020-2008-3

Yang, J. F., Wang, F., Chen, Y. Z., Hao, G. F., & Yang, G. F. (2020a). LARMD: Integration of bioinformatic resources to profile ligand-driven protein dynamics with a case on the activation of estrogen receptor. *Briefings in Bioinformatics*. https://doi.org/10.1093/bib/bbaa010

Yang, J. M., & Chen, C. C. (2004). GEMDOCK: A generic evolutionary method for molecular docking. *Proteins: Structure, Function, and Bioinformatics*, *55*(2), 288–304. https://doi.org/10.1002/prot.20035

Yang, S. N., Atkinson, S. C., Wang, C., Lee, A., Bogoyevitch, M. A., Borg, N. A., & Jans, D. A. (2020b). The broad spectrum antiviral ivermectin targets the host nuclear transport importin α/β1 heterodimer. *Antiviral Research*, *177*, 104760. https://doi.org/10.1016/j.antiviral.2020.104760

Yao, D., Cui, H., Zhou, S., & Guo, L. (2017). Morin inhibited lung cancer cells viability, growth, and migration by suppressing miR-135b and inducing its target CCNG2. *Tumour Biology*, *39*(10), 1010428317712443. Sephttps://doi.org/10.1177/1010428317712443

Yoon, J. H., & Baek, S. J. (2005). Molecular targets of dietary polyphenols with anti-inflammatory properties. *Yonsei Medical Journal*, *46*(5), 585–596. https://doi.org/10.3349/ymj.2005.46.5.585

Yoshida, M., Sakai, T., Hosokawa, N., Marui, N., Matsumoto, K., Fujioka, A., Nishino, H., & Aoike, A. (1990). The effect of quercetin on cell cycle progression and growth of human gastric cancer cells. *FEBS Letters*, *260*(1), 10–13. https://doi.org/10.1016/0014-5793(90)80053-L

Yoshimoto, F. K. (2020). The proteins of severe acute respiratory syndrome coronavirus-2 (SARS CoV-2 or n-COV19), the cause of COVID-19. *The Protein Journal*, *39*(3), 198–216. https://doi.org/10.1007/s10930-020-09901-4

Zhang, C., Wu, Z., Li, J. W., Zhao, H., & Wang, G. Q. (2020). The cytokine release syndrome (CRS) of severe COVID-19 and interleukin-6 receptor (IL-6R) antagonist tocilizumab may be the key to reduce the mortality. *International Journal of Antimicrobial Agents*, *55*(5), 105954. https://doi.org/10.1016/j.ijantimicag.2020.105954

Zhao, Y., Zhao, Z., Wang, Y., Zhou, Y., Ma, Y., & Zuo, W. (2020). Single-cell RNA expression profiling of ACE2, the putative receptor of Wuhan 2019-nCov. *BioRxiv*.

Zhou, P., Yang, X.-L., Wang, X.-G., Hu, B., Zhang, L., Zhang, W., Si, H.-R., Zhu, Y., Li, B., Huang, C.-L., Chen, H.-D., Chen, J., Luo, Y., Guo, H., Jiang, R.-D., Liu, M.-Q., Chen, Y., Shen, X.-R., Wang, X., … Shi, Z.-L. (2020). A pneumonia outbreak associated with a new coronavirus of probable bat origin. *Nature*, *579*(7798), 270–273. https://doi.org/10.1038/s41586-020-2012-7

Ziebuhr, J., Snijder, E. J., & Gorbalenya, A. E. (2000). Virus-encoded proteinases and proteolytic processing in the Nidovirales. *The Journal of General Virology*, *81*(Pt 4), 853–879. https://doi.org/10.1099/0022-1317-81-4-853

Zumla, A., Hui, D. S., Azhar, E. I., Memish, Z. A., & Maeurer, M. (2020). Reducing mortality from 2019-nCoV: Host-directed therapies should be an option. *The Lancet*, *395*(10224), e35–e36. https://doi.org/10.1016/S0140-6736(20)30305-6